Jan Rødal

On functional imaging and treatment planning for biologically adapted radiotherapy

Thesis for the degree of Philosophiae Doctor

Trondheim, March 2012

Norwegian University of Science and Technology
Faculty of Natural Sciences and Technology
Department of Physics

Oslo University Hospital
Norwegian Radium Hospital
Department of Medical Physics

NTNU – Trondheim
Norwegian University of
Science and Technology

Oslo
University Hospital

NTNU
Norwegian University of Science and Technology

Thesis for the degree of Philosophiae Doctor

Faculty of Natural Sciences and Technology
Department of Physics

ISBN 978-82-471-3400-9 (printed ver.)
ISBN 978-82-471-3401-6 (electronic ver.)
ISSN 1503-8181

Doctoral theses at NTNU, 2012:65

Printed by NTNU-trykk

Preface

This work was accomplished at Department of Physics, Faculty of Natural Sciences and Technology, Norwegian University of Science and Technology (NTNU), from September 2008 to December 2011 (full time position as medical physicist from July 2011). The experimental work was carried out at Department of Medical Physics, Norwegian Radium Hospital, Oslo University Hospital (OUS). The work was supported by Siemens AS, Norway, and Department of Medical Physics, OUS.

The main supervisor has been Professor Eirik Malinen, OUS. The academic supervisor has been Professor Arne Skretting, OUS and NTNU, until February 2011. He was followed by Professor Tore Lindmo, NTNU, from February 2011, due to Arne Skrettings retirement from his position at Department of Physics, NTNU.

Contributions

The papers included in this thesis are written in co-operation with several authors, who have all given written consents to the use of the papers. Eirik Malinen contributed significantly to the planning of the experiments and the data analyses. He is first author of paper I and contributed significantly to the data analysis for this paper. Åste Søvik and Hege Kippenes Skogmo contributed significantly to the imaging and treatment of the canine patients. Åste Søvik is first author of paper III and contributed significantly to the dose plan analysis for this paper. Ingrid Skjei Knudtsen contributed to the PET and CT acquisitions for paper I and II. Einar Waldeland contributed to the planning and experimental work of paper V, and Christoffer Lervåg and Karsten Eilertsen contributed to the data analysis in paper III. All co-authors were involved in the final stages of writing the papers.

Oslo, December 2011.

Jan Rødal

Acknowledgements

My main supervisor, Professor Eirik Malinen, is greatly acknowledged for his ever enthusiastic supervision and support of my work for this thesis, and for always being available for discussions. I highly appreciate your extremely positive attitude and the effort you have put into the projects.

I am thankful to my academic supervisors, Professor Arne Skretting and Professor Tore Lindmo, for their support of my work and for being links to the Faculty of Natural Sciences and Technology. Vidar Jetne and Karsten Eilertsen at The Department of Medical Physics are highly acknowledged for the practical arrangements of my position and the financial support of the work.

I also wish to express my gratitude to my co-workers Åste Søvik, Hege Kippenes Skogmo, Ingerid Skjei Knudtsen, Einar Waldeland and Christoffer Lervåg for their positive attitude and professional contributions to the results, and to Dag Rune Olsen and Øyvind Bruland for participating in the initiation of my PhD project. I have enjoyed our interesting disciplinary discussions, but also the off-topic talks concerning matters like sport dogs and ballistics, which have shortened the wait during PET imaging and treatments. My colleagues at the Department of Medical Physics are also highly appreciated for contributing to a great job environment.

Special thanks to the Section of Nuclear Medicine for supporting the projects, and to the staff at the PET/CT and the treatment machine for their enthusiastic participation. Thanks also to the veterinary students who have handled the canine patients, spending almost 40 of their valuable evenings at the hospital.

Finally, warm thoughts to my wife, Heidi, for being supernaturally positive minded and for giving crucial disciplinary feed back in reading my thesis and papers.

List of papers

I. Malinen E, Rødal J, Knudtsen IS, Søvik Å, Skogmo HK. Spatiotemporal analysis of tumor uptake patterns in dynamic ^{18}FDG-PET and dynamic contrast enhanced CT. *Acta Oncologica* 2011;50:873-882.

II. Rødal J, Søvik Å, Skogmo HK, Knudtsen IS, Malinen E. Feasibility of contrast-enhanced cone-beam CT for target localization and treatment monitoring. *Radiotherapy and Oncology* 2010;97:521-524.

III. Søvik Å, Rødal J, Skogmo HK, Lervåg C, Eilertsen K, Malinen E. Adaptive radiotherapy based on contrast enhanced cone-beam CT imaging. *Acta Oncologica* 2010;49:972-977.

IV. Rødal J, Søvik Å, Malinen E. Influence of MLC leaf width on biologically adapted IMRT plans. *Acta Oncologica* 2010;49:1116-1123.

V. Rødal J, Waldeland E, Søvik Å, Malinen E. Dosimetric verification of biologically adapted IMRT. *Medical Physics* 2011;38:2586-2594.

Summary

Tumours show large variations in response to radiotherapy, both across tumour types and within individual tumours. One way to counteract radioresistance is to increase the radiation dose to resistant regions by so-called biologically adapted therapy. Visualisation of these regions based on properties related to radioresistance, such as metabolism, hypoxia, proliferation, and vascularisation, can act as basis for target definition, and can be obtained by PET/CT, dynamic MRI, and dynamic CT imaging.

One aim of the present work was to improve tumour visualisation in images obtained before and during radiotherapy. An analysis of dynamic FDG-PET (D-PET) and dynamic contrast-enhanced CT (DCE-CT) images of three canine patients showed similarities between the two image modalities with respect to tumour vascularisation. The results indicated that D-PET may be used alone for assessment of both tumour perfusion and metabolic activity, simplifying the image acquisition. We also investigated a new method for tumour visualisation by use of image subtraction in CE cone-beam CT (CE-CBCT) images, obtained during IMRT of one of the dogs. The method was shown to be feasible and produced images with a clearly visualised tumour.

We further aimed to investigate the radiobiological effect of biologically adapted dose delivery. An IMRT planning study based on CE-CBCT images of the first canine IMRT patient demonstrated that such dose planning was feasible. This approach gave the highest effect on the tumour and thus showed that biologically adapted treatment was the best choice for this treatment case. Furthermore, a hypoxia dose painting study with a highly heterogeneous tumour model, where MLC leaf widths and IMRT parameters were varied, indicated that reducing the leaf widths from 10 to 5 or 2.5 mm gave increased tumour control probability. We also implemented dose painting by contours in an anthropomorphic phantom. An optimal dose delivery was not achieved.

In conclusion, dynamic FDG-PET before radiotherapy and CE-CBCT during radiotherapy may be valuable. Dose painting should preferably be delivered by MLCs with small leaf widths. However, a high radiobiological effect from high-resolution dose painting could not be demonstrated in practice. An alternative dose painting approach or treatment modality may thus be required for biologically adapted dose delivery to highly heterogeneous tumours.

Table of contents

Abbreviations

3-D	Three-dimensional
^{64}Cu-ATSM	^{64}Cu-methyl-thiosemicarbazone
Bq	Becquerel
BTV	Biological target volume
CBCT	Cone-beam CT
CE	Contrast-enhanced
CIN	Contrast-induced nephropathy
CRT	Conformal radiotherapy
CT	Computed tomography
DCE-CT	Dynamic contrast-enhanced CT
DCE-MRI	Dynamic contrast-enhanced MRI
DICOM	Digital Imaging and Communications in Medicine
DNA	Deoxyribonucleic acid
DPBC	Dose painting by contours
DPBN	Dose painting by numbers
D-PET	Dynamic PET
ECM	Extracellular matrix
EDR	Extended dose range
EES	Extravascular, extracellular space
EF5	2-(2-Nitro-1*H*-imidazol-1-yl)-*N*-(2,2,3,3,3-pentafluoropropyl)acetamide
EGFR	Epidermal growth factor receptor
EPID	Electronic portal imaging device
EUD	Equivalent uniform dose
FAZA	^{18}F-azomycin-arabinoside
FDG	^{18}F-fluoro-2-deoxyglucose
FET	Fluoroethyl-L-tyrosine
FETA	^{18}F-fluroetanidazole
FETNIM	^{18}F-Fluoroerythronitroimidazole
FLT	^{18}F-fluorothymidine
FMISO	^{18}F-fluoromisonidazole
Gd-DTPA	Gadolinium diethylene triamine pentaacetic acid
GLUT	Glucose transporter
Gy	gray
GTV	Gross target volume

HIF	Hypoxia-inducible factor
HK	Hexokinase enzyme
HR	Homologous recombination
IGRT	Image guided radiotherapy
IMAT	Intensity modulated arc therapy
IMRT	Intensity modulated radiotherapy
iv	Intravenously
LQ	Linear-Quadratic model
LSO	Lutetium oxy-orthosilicate
MET	Methyl-methionine
MLC	Multileaf collimator
MMP	Metalloproteinase
MR	Magnetic resonance
MRI	Magnetic resonance imaging
MRS	Magnetic resonance spectroscopy
NARA	Norwegian Animal Research Authority
NHEJ	Nonhomologues end joining
NMR	Nuclear magnetic resonance
NTCP	Normal tissue complication probability
OER	Oxygen enhancement ratio
PET	Positron emission tomography
PMMA	Polymethyl methacrylate
pO_2	Partial pressure of oxygen (O_2)
PO_4	Phosphate
PTV	Planning target volume
RF	Radio frequency
SF_2	Survival fraction at 2 Gy
SPECT	Single-photon emission CT
SUV	Standard uptake value
T1, T2	Time constants in MRI
TCP	Tumour control probability
TOF	Time-of flight
VMAT	Volumetric modulated arc therapy
VSIM	Virtual simulator
XVI	X-ray volume imaging

1. Introduction

Solid tumours are heterogeneous and structurally complex with respect to factors like blood flow, oxygen and nutrient supply, cell growth, cell density, pH, and bioenergetic status.[1, 2] These biological factors are primarily created by inadequate and heterogeneous vascular networks, and give rise to a variable resistance to nonsurgical treatments like chemotherapy and radiotherapy. The variability in such resistance factors exists both between and within tumour types, between different parts of the tumour, and may also change with time.

Radioresistant cells within a tumour may cause recurrent growth and thus lack of local control following therapy.[3-5] It has therefore been suggested to apply heterogeneous tumour dose distributions in accordance with the spatial and temporal variation of radiosensitivity, so-called biologically adapted radiotherapy.[6-14] To guide such focal dose escalation, a radioresistance map of the tumour is required. One strategy to obtain such a map is through noninvasive biological imaging.

Biological imaging includes molecular imaging, which deals with the cellular and sub cellular biological processes, and functional imaging, which focuses on physiological activities within a certain tissue.[15, 16] Advances in these modalities may improve our ability to depict targets which may reflect the radioresistance of the tumour. Through functional imaging with computed tomography (CT), magnetic resonance imaging (MRI), and positron emission tomography (PET) one can visualise factors like vasculature, proliferation, hypoxia, and metabolism.[17] These characteristics may serve as guidance maps for focal dose escalations in radiotherapy. Assessment of such factors before, during and after treatment is thus important to tailor personalised treatment regimens.[18] It is still a matter of discussion, however, how to best incorporate this information into radiotherapy and the literature shows that there is high interest in this field.[19]

Technological developments in radiotherapy, such as inverse treatment planning algorithms, intensity modulated radiotherapy (IMRT), and multileaf collimators (MLCs) with increased resolution and accuracy have enabled high gradient,

heterogeneous dose distributions in the patient. Such achievements have therefore been a premise for implementing focal dose escalation. The width of the MLC leafs influences the obtainable resolution of the dose distributions, and has been widely investigated in modelling studies.[19, 20] Data concerning biological effect evaluations for various leaf widths are still scarce, though, and the optimal resolution for biologically adapted therapy is yet to be decided.[21]

Cone-beam CT (CBCT) has been integrated with the linear accelerator for volumetric imaging in the therapy room, and has contributed highly to the development of image guided radiotherapy (IGRT). Visualisation of tumour related changes during treatment is of great interest for treatment setup and monitoring. Still, soft tissue components may be hard to separate in cone-beam CT images. Improving tumour to background contrast in cone-beam imaging may be advantageous in biologically adapted radiotherapy.

2. Aims

The overall aims of this study were to improve tumour visualisation and to investigate the radiobiological effect of biologically adaptive dose delivery.

Specific aims were to:

- Compare early uptake patterns obtained by dynamic ^{18}F-fluoro-2-deoxyglucose (FDG) PET and dynamic contrast-enhanced CT (DCE-CT) imaging (paper I).

- Investigate the feasibility of using contrast-enhanced CBCT (CE-CBCT) to visualise the tumour before and during treatment, and evaluate different treatment adaptation strategies based on such visualisation (paper II and III).

- Analyse the effect of radiotherapy planning with different MLC leaf widths and investigate the delivery of biologically adapted heterogeneous dose distributions to an anthropomorphic phantom (paper IV and V).

3. Background

3.1. Cancer

Tumour and neoplasm are collective terms denoting an abnormal mass of tissue resulting when cells with changed or damaged genetic material (DNA) begin to grow without control.[22] Cells from benign tumours do not spread to other parts of the body, and can often be removed without coming back, they are not cancerous. Malignant tumours, however, are cancerous, and lead to significant morbidity and mortality. They grow into surrounding normal tissues and metastasise to vital organs throughout the body.[23] Such distant spread of tumour cells is the cause of 90% of human cancer deaths.[24, 25] It has been proposed that the genetic characteristics, or genotypes, of cancer cells are manifested in six essential alterations in the cell physiology, acquired during tumour development: self-sufficiency in growth signals, insensitivity to antigrowth signals, evasion of programmed cell death, or apoptosis, unlimited growth potential, sustained blood vessel growth, and tissue invasion and metastasis.[25] Later progress has further added two emerging hallmarks to this list; reprogramming of energy metabolism and evading immune destruction (Fig. 1).[26] There are more than 100 different cancer types, usually named by the body site where they originated.[27] Some cancers start in blood cells and do not give rise to tumours, while cancers arising from organs and solid tissues become solid tumours. The latter represents more than 90% of all human cancers.[22, 23]

Among the 4,9 million inhabitants in Norway, there were registered 27 520 new cancer cases in 2009 (0.6%), and 10 600 patients received external radiotherapy.[28] A total of 200 000 persons had cancer in 2009 (4%), and the probability of developing cancer before the age of 75 is 28% in women and 35% in men.[29] The cancer incidence in Norway has been increasing since population-based cancer surveys were initiated. In the period 2004-2009 the general increase in incidence was 1.8% per year, but the number varies highly between cancer types. The five-year survival also varies much between cancer types and was around 14% for lung cancers, 63% for colon and rectum

cancers and 87% for prostate and breast cancers (2004-2009). These numbers show an increase of 2-8% from the previous five year period.

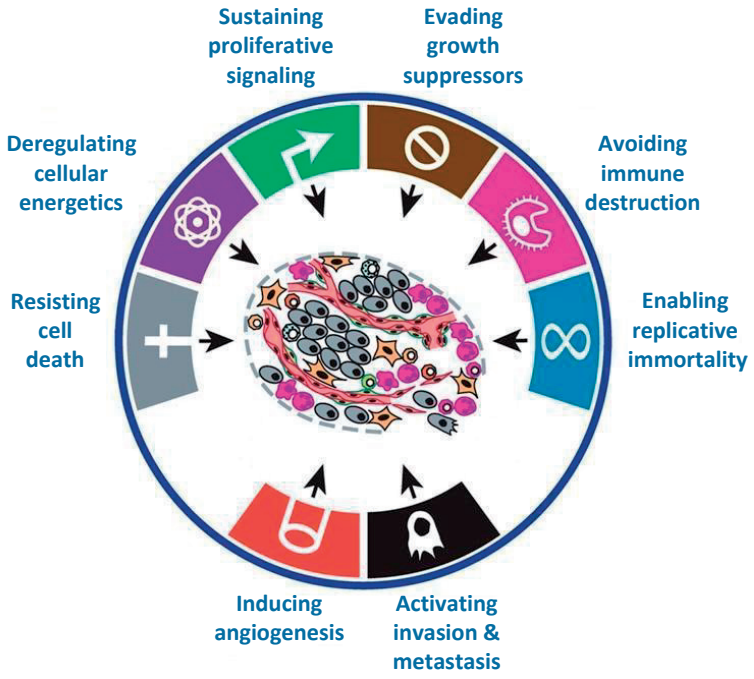

Figure 1. *The eight hallmarks of cancer. Adapted from Hanahan and Weinberg.*[26]

Tumour vasculature

To grow beyond a small pool of tumour cells and induce metastatic spread, the cancer has to develop its own blood supply.[30] This is done by stimulating the growth of endothelial cells from surrounding vessels into the tumour, a process known as angiogenesis.[23] These newly formed blood vessels are highly different from normal vasculature. They are irregular and tortuous with branching patterns that feature excessive loops, blind ends and arteriolar-venous shunts, and they tend to be more leaky (Fig. 2).[1] These vessel structures result in disorganised and variable blood flow, making the delivery of oxygen and nutrients to the tumour cells less efficient than in normal tissues. This leads to acidic, glucose- and oxygen-deprived regions in most tumours.

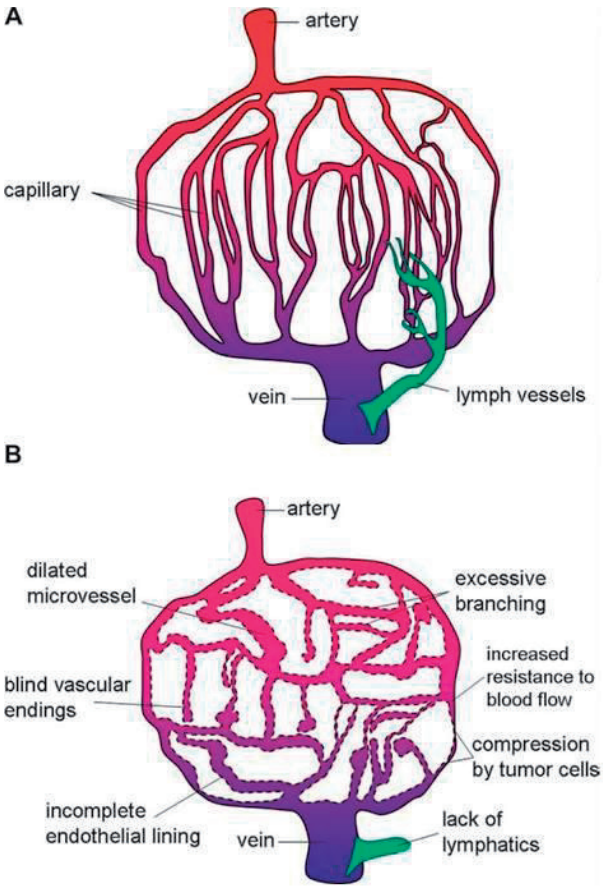

Figure 2. *The vascular system in normal tissue (A) and in solid tumour (B).*[1]

Hypoxia

Normal tissues typically have a median oxygen pressure of 40-60 mmHg (pO_2).[23] Tumour tissues with severely reduced oxygen concentration are termed hypoxic. They may even be completely depleted of oxygen, i.e. anoxic. Diffusion-limited, or chronic, hypoxia increases with distance between the nutritive blood vessel and the tumour cells. A distance of more than roughly 50 μm can give pO_2 values lower than 2.5 mmHg.[31] The cells are still viable, but with increasing distance to the vessel they will eventually

die and necrotic tissue will develop. Blood vessels may also be temporarily occluded, leading to perfusion-limited O_2 delivery. This is often a transient condition and may be termed acute hypoxia.[32]

It has been shown that 50-60% of locally advanced solid tumours can exhibit hypoxic and anoxic regions that are heterogeneously distributed within the tumour masses.[32] It has also been indicated that hypoxia-adapted cells can proliferate despite oxygen or nutrient deprivation.[33] This may lead to increased potential for local invasive growth and regional and distant spread.[2, 31] This hypoxia-driven, malignant progression may result in an aggressive and treatment resistant tumour phenotype.

Canine tumours

Naturally occurring canine cancers are attractive models in oncology.[18] They share many features with human cancers, including histological appearance, tumour genetics, molecular targets, biological behaviour, and response characteristics to conventional therapies.[34] Tumours in pet dogs are comparable in size to human tumours, and are relatively outbred compared with tumours in small laboratory animals like mice and rats. The canine genome also shows closer similarities with human genomes in those gene families associated with cancer compared with for example the mouse genome. The range of cancers in pet dogs is as diverse as the cancers seen in human patients and have the same biological features, including tumour vasculature and hypoxia, metastatic capacity, acquired resistance to therapy, and recurrence rate.[34]

3.2. Radiobiology

The use of x-rays for treatment of cancer, and a large number of nonmalignant conditions, was started quite immediately after the discovery of x-rays in 1895. It was quickly realised, however, that the radiation dose could not be increased indefinitely due to the toxic effects to normal tissues. Radiotherapy is therefore beneficial only if the tumour response occurs at a total cumulative dose that does not result in severe normal tissue complications. This led to the concept of the therapeutic window. This concept describes the response of the tumour and normal tissues as a function of cumulative

dose for fractionated radiotherapy (Fig. 3). A certain dose difference must exist between the two response curves for the treatment to be beneficial.

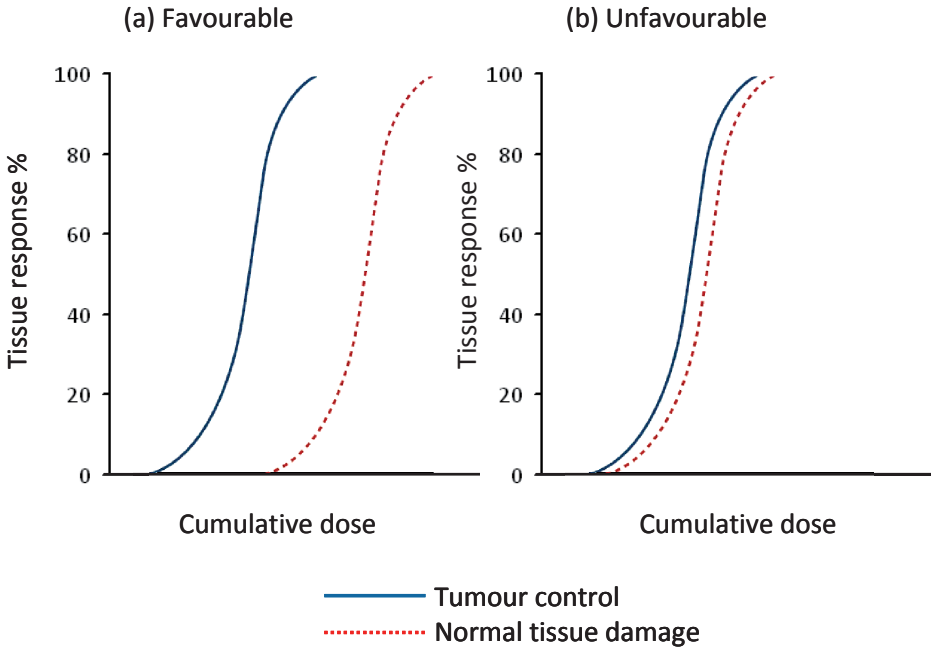

Figure 3. *(a) The therapeutic window is large when the response of tumour tissue is greater than that of normal tissue. (b) The therapeutic window is small when the response is similar. Adapted from Bernier* et al.[35]

Different radiobiological experiments were carried out during the first decades of the 20th century, and in the middle of the 1920s these investigations started to have an considerable impact on the design of radiotherapy.[35] In the 1930s a consensus emerged that it was favourable to divide one large single-dose treatment into a series of low-dose treatments, known as fractionated radiotherapy. The treatment effect could then be achieved with less damage to normal tissues. 20 years later, in 1953, Louis Harold Gray showed that the sensitivity of tumour cells to radiation was higher under well-oxygenated conditions than under hypoxic conditions.[36] This time period thus led to the identification of the radiobiological factors that influence the response to fractionated treatments, known as the four Rs of radiotherapy: Repair, Repopulation, Redistribution and Reoxygenation.[37]

Repair

Normal cells proliferate relatively slowly and have time to repair radiation induced DNA damages before replication. Conversely, rapidly proliferating tumour cells may undergo DNA replication with unrepaired damages, which can be lethal. Fractionated radiotherapy is thus essential for normal tissue repair and contributes to an increased therapeutic window when normal tissues proliferate more slowly than the tumour.

Repopulation

Tumour cells that survive irradiation may proliferate, or repopulate, which is a negative effect from fractionation. Splitting the treatment into many fractions over an extended treatment period may further induce *accelerated* proliferation of the surviving tumour cells. This increases the number of cells to be killed and prolonged treatment times may therefore reduce the possibility to achieve local control. Sufficient time between fractions is anyhow essential for the normal cells to repair sublethal damage, and 4-6 hours between fractions seems to be an adequate interval.

Redistribution

Cells are more resistant to radiation when they are in the S-phase of the cell cycle. Most surviving cells will thus be in this phase. Allowing time for these cells to progress into another, more sensitive phase and then be irradiated again is therefore an argument for fractionated radiotherapy.

Reoxygenation

Another beneficial effect of fractionation is the reoxygenation of hypoxic tumour cells. After irradiation the hypoxic fraction of tumour cells is increased due to the inactivation of the more radiosensitive aerobic cells. Reoxygenation of the hypoxic cells will occur after irradiation, however, gradually increasing the tumour radiosensitivity. The reoxygenation occurs over a time span from a few hours to several days, depending on the underlying mechanisms.

Altered fractionations

In conventional fractionation, a fraction dose of 1.8-2.0 Gy is delivered to the tumour once a day, five days a week. Many locally advanced diseases cannot be controlled by

this regimen and alternative schedules have been derived from laboratory and clinical observations made in the 1970s and 1980s.[35] These studies showed that giving smaller and more frequent fractions allowed for higher total doses without causing increased late morbidity in normal tissues. This approach is termed hyperfractionation.

Many tumours show rapid cell proliferation, which may even be accelerated by irradiation. Shortening of the treatment time to counteract this repopulation is thus justified and is the rationale behind accelerated fractionation. Accelerated fractionation implies a reduced overall treatment time and an increased mean dose per week above the 9-10 Gy given in conventional fractionation.[37] Both hyperfractionation and accelerated fractionation have been shown to give significant survival benefits. For example as shown in a large meta-analysis of 6515 patients with head and neck cancers, where a survival benefit of 8% was found for hyperfractionation, and 2% for accelerated radiotherapy.[38]

3.3. Tumour radioresistance

Due to the heterogeneity in biological factors, cancers show large variations in radioresistance and respond differently to radiotherapy. Tumour types like melanoma, osteosarcoma and glioblastoma are in general among the radioresistant ones, while lymphoma, myeloma and neuroblastoma are among the most radiosensitive[37]. Different types of carcinomas and lung cancers lie in between, but may also be very radioresistant in certain cases. Tissue radiosensitivity is determined mainly by three mechanisms; intrinsic radioresistance, tumour cell proliferation, and hypoxia.[2, 31, 39, 40] Visualisation of radioresistant cells based on these processes thus constitutes the principal foundation for dose escalation in radiotherapy.

Intrinsic radioresistance

Intrinsic radioresistance is a result of the enzymatic repair of double-strand breaks and other DNA damage induced by radiation. Tumour cells can show an increased DNA repair capacity which will influence the outcome of radiotherapy.[40] This is confirmed for example by the positive expression of repair enzymes and reduced clinical response and survival in cervical cancer.[41-43] It is further shown that tumour cell radiosensitivity

is a significant and independent prognostic factor for the outcome of radiotherapy for cervix and head and neck carcinomas.[44-46] Intrinsic radiosensitivity was here measured by the survival fraction at 2 Gy *in vitro* (SF_2), i.e. without the influence of hypoxia and repopulation effects.

Homologous recombination (HR) and nonhomologous end joining (NHEJ) are two main pathways involved in repair of double strand breaks, and several gene therapy strategies have been developed to inhibit such pathways.[37] However, DNA therapy has not yet gained widespread clinical implementation, as is also the case for other therapies based on antibodies targeting repair enzymes. Increasing the irradiation dose by hyperfractionation is so far the chosen strategy for overcoming intrinsic radiosensitivity. Combinations with chemotherapy have been found beneficial, for example in advanced laryngeal cancer.[47]

Proliferation

Tumours with rapid proliferation show high radioresistance due to the increased growth between sessions of fractionated radiotherapy. A retrospective review of nearly 500 head and neck cancers concluded that increased proliferation set in after a certain treatment time, 3-4 weeks in the referred case. An increase in total dose of 0.6 Gy per day prolonged treatment time was required as compensation.[48, 49]

Activation of the epidermal growth factor receptor (EGFR) is one pathway for cells to enhance their proliferation in response to radiotherapy or chemotherapy.[50] It has therefore been proposed to combine radiotherapy with EGFR-targeted cytostatic agents, for example cetuximab, to inhibit repopulation and thereby increase the radiation response.[40, 50] Results from such studies have been promising for tumour control, but have also increased normal tissue toxicity. Another approach is accelerated radiotherapy which has shown increased loco-regional control in treatment of head and neck cancers, and of Burkitt's lymphoma.[38, 47, 50] Chemotherapy in combination with radiotherapy has also been shown to give improved survival in primary treatment of head and neck and cervix cancers, possibly due to the inhibition of tumour cell repopulation.[50]

Hypoxia

Radioresistance to electron and photon radiation rapidly increases when pO_2 in a tumour is reduced below 25-30 mm Hg (Fig. 4).[2]

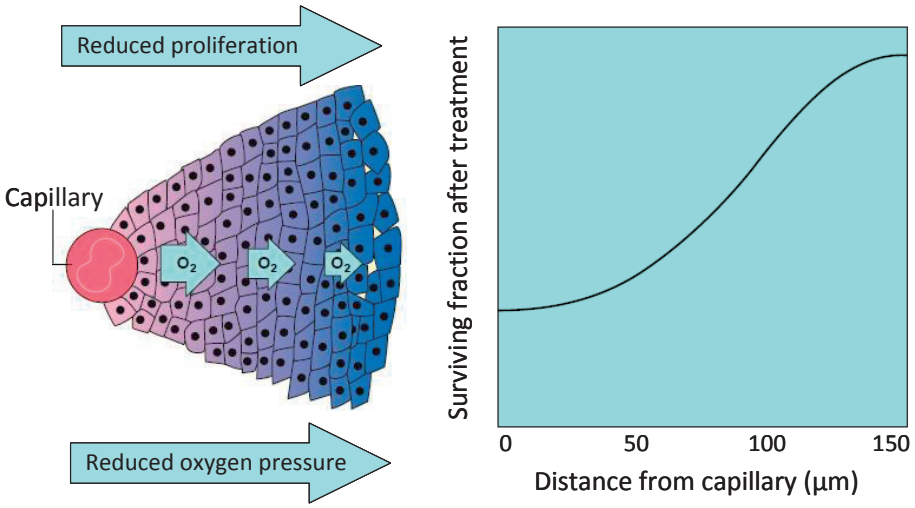

Figure 4. *(Left) Part of a tumour surrounding a capillary. The partial oxygen pressure decreases with increasing distance from the capillary. (Right) This reduces the cell kill in response to radiation and anticancer drugs. Adapted from Brown.*[23]

The increased radioresistance is caused by two main mechanisms:

- Reduction of the *direct* oxygen-enhancement effect, with fewer fixations by oxygen of the radiation induced free radicals in the DNA structure. If oxygen is not present during irradiation, the damaged molecules can be restored to their original form by reaction with H^+.[44] For most cell types, the oxygen enhancement ratio (OER) for x-rays is around 3, but may be lower than this at radiation doses below 3 Gy.[36, 44]

- The *indirect* radioresistance is caused by selection of tumour subpopulations surviving the hostile hypoxic environment. These clones may have hypoxia-induced genetic changes leading to lower apoptotic potential and higher proliferation rate, representing a more aggressive tumour type with increased radioresistance.[2] Additionally, hypoxia results in an increase in DNA repair enzymes and radical scavengers, also leading to decreased cell death.[51]

It has been shown that hypoxia, measured by polarographic electrodes, is an independent prognostic factor which indicates significantly lower loco-regional control after radiotherapy of head and neck cancers.[52] The same has been shown for uterine cervical cancers and soft tissue sarcomas.[2, 53] The use of the hypoxia radiosensitiser nimorazole in the DAHANCA 5 head and neck study is an example of counteracting the direct oxygen-enhancement effect.[54] Patients with low plasma osteopontin levels, as a marker of low degree of hypoxia, showed significantly improved loco-regional control and disease-specific survival.

The adverse prognostic impact of hypoxia may, however, also be caused by increased regional and distant metastatic potential of these tumours.[2] It is important to note that such properties can not be altered by local doses of radiation.

3.4. Tumour response modelling

Tumour control probability

Radiobiological experiments have demonstrated that the survival of irradiated cells can be described by the Linear-Quadratic (LQ) model of cell killing:

$$S = e^{-\alpha d - \beta d^2} = e^{-\alpha d\,(1+\frac{\beta}{\alpha}d)} \qquad (1)$$

where S is the surviving fraction after a dose d of radiation to a population of cells.[37, 55-57] α and β characterise the initial slope and curvature, respectively, of the survival curve. For a fractionated treatment course with n fractions of dose d each, the expected number N_s of surviving, clonogenic cells is thus given by:

$$N_s = N_0 S^n = N_0 e^{-\alpha n d\,(1+\frac{\beta}{\alpha}d)} \qquad (2)$$

where N_0 is the initial number of clonogenic cells. Cell repopulation rate and the reoxygenation effect are here not taken into account. Repopulation may

straightforwardly be taken into consideration, however, by adding a γT term in the exponent, where γ is the repopulation rate and T is the overall treatment time.

Tumour eradication is only obtained when every single clonogenic cell has been eliminated, i.e. when N_s in equation (2) is zero. The probability that no single clonogenic cell is present if the mean number of clonogenic cells is N_s can be obtained from Poisson statistics:

$$P(N_S, y) = \frac{e^{-N_S} {N_S}^y}{y!} \tag{3}$$

which gives the probability P of the occurrence of exactly y events when the mean number of events is N_S. The tumour control probability (TCP) corresponds to the probability of finding zero surviving cells, i.e. when $y = 0$:

$$TCP = P(N_S, 0) = e^{-N_S} \tag{4}$$

The clinical implication of this formalism may be illustrated by an example of a massive tumour reduction from 10^9 clonogens down to a mean of 4. The surviving fraction is here as low as $4 \cdot 10^{-9}$, but the TCP is still only $e^{-4} = 1.8\%$. Increased cell killing by a factor 100 reduces the mean number of surviving cells to 0.04, leading to TCP = 96%. These examples indicate that eradicating all the cells in a tumour is a demanding challenge. The TCP value may be very useful as a relative measure, as for example in comparing dose plans and in evaluating the effects of changing parameters in plans. The absolute TCP values must be treated with great caution, however, due to the lack of clinical data on radiosensitivity and clonogenic cell density.[55]

For a tumour with volume V and clonogenic density ρ_0 the probability of not finding any surviving clonogens, and thus obtaining tumour control, is from equations (2) and (4) given by:

$$TCP = e^{-\rho_0 V S^n} = e^{-\rho_0 V e^{-n\alpha d\left(1+\frac{\beta}{\alpha}d\right)}} \tag{5}$$

From a radiobiological point of view, this equation is fundamental for the understanding of tumour response and its influencing factors. It states, for example, that the relative importance of the intrinsic radiosensitivity, given by α and β, is greater than that of the clonogenic density, ρ_0.

In the case of nonuniform dose distributions in the target volume, the tumour may be divided into a number of independent subunits. If the tumour consists of N such subvolumes, the control probability for a given subvolume is:

$$TCP_i = e^{-\rho_{0,i} V_i e^{-n\alpha_i d\left(1+\frac{\beta_i}{\alpha_i}d\right)}} \tag{6}$$

where V_i is the volume of element i. V_i may for voxel-wise representation of the tumour be considered to be a constant V_{vox} equal to the voxel volume. Finally, the total cure probability is the product of the cure probabilities for each subvolume of the tumour:

$$TCP = \prod_{i=1}^{N} TCP_i = e^{-\sum_{i=1}^{N} \rho_{0,i} V_i e^{-n\alpha_i d\left(1+\frac{\beta_i}{\alpha_i}d\right)}} \tag{7}$$

There is large inter-patient heterogeneity in the intrinsic radiosensitivity of the tumour cells, i.e. in the α values, and this is suggested to be the main cause for clinically observed TCP response curves being less steep.[55, 56] This inter-patient variation is suggested to have a larger impact than the radiosensitivity variations between clonogenic cells within each tumour, i.e. the intra-patient variation.[55] It is therefore warranted to have a population-based TCP, which may be defined as:

$$TCP_{pa} = \int_0^{\infty} \left(\prod_{i=1}^{N} TCP_i \right) g(\alpha) d\alpha \qquad (8)$$

where g(α) is the frequency distribution of α, which may be assumed to follow a Gaussian distribution.

Another concept concerning dose-response relationships in radiotherapy is the normal tissue complication probability (NTCP). The NTCP describes the effects on normal tissues for partial-volume irradiations and inhomogeneous dose distributions, and different models have been proposed for this purpose.[37] The concept has, however, not been dealt with in the present work and will therefore not be further outlined.

Equivalent uniform dose

The concept of equivalent uniform dose (EUD) is relevant when the dose is distributed inhomogeneously over the target volume. The formalism converts the inhomogeneous dose distribution into a single dose, the EUD, which causes the same radiobiological effect when distributed uniformly over the target volume.[44, 58] In terms of cell kill, the EUD may be defined as:

$$e^{-n\alpha EUD\,(1+\frac{\beta}{\alpha}EUD)} = \frac{1}{N}\sum_{i=1}^{N} e^{-n\alpha d_i (1+\frac{\beta}{\alpha}d_i)} \qquad (9)$$

The right-hand side of the equation describes the mean surviving fraction over N voxels, where each voxel receives a dose d_i. The left-hand side describes a situation where all voxels have been irradiated with a dose EUD. This gives an equation quadratic in EUD, with the physical solution (for EUD>0):

$$EUD = \frac{-\alpha + \sqrt{\alpha^2 - \frac{4\beta}{n}\ln\left[\frac{1}{N}\sum_{i=1}^{N} e^{-n\alpha d_i (1+\frac{\beta}{\alpha}d_i)}\right]}}{2\beta} \qquad (10)$$

While the TCP is a parameter which gives the probability of reaching a certain endpoint, i.e. the probability of eradicating the tumour, the EUD gives a dose as output. The EUD can thus be compared with for example the prescribed target dose, or a dose limit for a risk organ.

3.5. Medical imaging

The first clinical images obtained by CT and MRI were taken in 1971 and 1976, respectively, and commercial installations of these imaging systems were available a few years later.[59,60] Parallel to the progress in CT and MRI imaging, the PET was developed and clinical use of the first practical PET scanner was published in 1975.[61] The development of radiopharmaceuticals, in particular FDG, contributed heavily to the entry of PET imaging into medicine.[62] Later, in 2001, a dual mode PET/CT scanner was commercially introduced which integrated the PET and CT modalities into one device.[63]

CT and MRI have the advantage of high anatomical and temporal resolution, and they are supplementary in their visualisation of tissue types. By including contrast agents one can also depict tumour perfusion and diffusion into the extravascular, extracellular space (EES). Functional information about tumour vasculature can thus be obtained. CT and conventional MRI do not map processes like metabolism and proliferation, and no information can be obtained about tissue viability.[64]

PET imaging has, by contrast, low anatomical resolution, but provides biological insights about the tumour tissue, such as metabolism, proliferation and oxygen status. A broad range of isotope markers incorporated into biological molecules have been developed for PET imaging of these processes, and the modality has become a complementary technique to CT and MRI.

CT

CT images are constructed on the basis of transmission measurements of a fan-shaped x-ray beam which rotates around the patient. The distribution of attenuation coefficients within the depicted volume is calculated by means of digital reconstruction algorithms, and each element, or pixel, of the CT image is thereby assigned a CT number. The CT numbers appear as grey values in the images and are presented in Hounsfield units

(HU), which relate the linear attenuation coefficient in each voxel to the attenuation in water:

$$H = \frac{\mu_{tissue} - \mu_{water}}{\mu_{water}} \times 1000 \qquad (11)$$

where μ is the linear attenuation coefficient. The CT numbers range from -1000 for air up to between 700 and 3000 for different types of bone, with that for water set to 0.[65]

In dose planning systems, the patient tissue distribution is represented by a CT image series; a three-dimensional (3-D) CT matrix. Accurate photon beam dose computational methods rely on knowledge of the electron densities in this matrix.[66] Since the CT numbers bear a linear relationship to the attenuation coefficients, the properties in each volume element, or voxel, of the density matrix may be derived from the pixel values in the CT images.[67] Such density information is not provided by other imaging methods like MRI and PET. CT information is therefore essential to dose planning when the inhomogeneity of the irradiated medium is taken into account in the dose calculations.

The CT technology has evolved dramatically over the last decade. Helical scanners with multi detector rows, which scan continuously while the patient is moved through the CT gantry, were introduced in 1998, and in 2004 scanners with acquisition of 64 slices per rotation were introduced.[68] Such scanners now have a resolution below 0.5 mm and X-ray tube rotation times down to 0.3 s. These developments also made tumour perfusion measurements readily accessible, enabling functional evaluation of tissue vascularity through DCE-CT.[69]

Following injection of a contrast medium in the patient, DCE-CT applies repeated acquisitions of CT images over a selected volume. The changes in tissue density over time can then be measured from the distribution of contrast medium in the tumour. A contrast enhancement may also be observed from the leakage of contrast medium into the extravascular space. This is due to the contrast molecules having a relatively low molecular weight, up to 1550 Da for the contrast agents used in the present work, and due to tumours often demonstrating increased capillary permeability and vascular density over normal tissues. The contrast agents are further both hydrophilic and inert and are thus excluded from the intracellular space.

The usefulness of DCE-CT within oncology is related to vascularisation and tumour hypoxia. The functional information can quantify physiological changes of the tumour, which can aid in tissue characterisation, provide prognostic information, and produce clearer delineation of tumours, with corresponding benefits for radiotherapy planning.[30, 69]

MRI

While CT relies on ionising radiation for image generation, MRI utilises the principles of nuclear magnetic resonance (NMR) to generate sectional images. The NMR principle involves the interaction of atomic nuclei with imposed magnetic fields, which cause radio frequency NMR signals.[70] For NMR the atomic nuclei must have a magnetic moment and this presupposes a net nuclear spin.

The most common magnetic nucleus in tissues is the hydrogen nucleus, which is a single proton, and diagnostic imaging applications of NMR almost exclusively involve the hydrogen atom. Bone has a relatively poor hydrogen concentration and is therefore poorly displayed. The hydrogen content in soft tissue molecules yields, in contrast, excellent separation of for example water, fat, proteins and carbohydrates. These components are not so well separated in CT, and MRI and CT are therefore supplementary to each other concerning anatomical imaging.

The image contrast in MRI is determined by the NMR signal strength, which is influenced by the proton density and the T1 and T2 relaxation times. The influence of these parameters is determined by the pulse sequence settings, which aim at optimising the contrast in the tissue of interest. If the tissue contrast depends on differences in T1 times, the pulse sequence is termed T1 weighted, while T2 weighted sequences express tissue differences in T2 times.

Analogous to the CT modality, dynamic contrast enhancement is also applicable for MRI studies. DCE-MRI is conducted by injecting a paramagnetic contrast agent, for example Gd-DTPA, followed by repeated image acquisitions of a selected volume after the injection. The temporal changes in tissue contrast can then be measured and analysed. As tumour oxygenation is dependent on the vascularisation, this is a proposed method for evaluating tumour hypoxia, as for CT.[71]

MR scanners may also provide diffusion weighted imaging and magnetic resonance spectroscopy (MRS). Such imaging capabilities are of minor relevance for the current work and will not be further outlined here.

PET

PET is a nuclear medicine imaging technique that makes use of positron emitting isotopes such as ^{11}C, ^{13}N, ^{15}O and ^{18}F. The isotopes are incorporated into biological molecules which act as tracers. The tracers have equal or similar chemical forms as naturally occurring biological substrates and can be taken up by cells. The emitted positrons slow down to thermal equilibrium in the tissue and recombine with electrons. This happens in a few picoseconds after emission and results in pairs of 0.511 MeV annihilation photons, emitted in opposite, collinear directions and registered in a 360° detector array around the patient. The positrons have a mean travelling distance of up to 1 mm in tissue and together with a small non-co-linearity in the order of 0.25° for the annihilation photons, this affects the obtainable spatial resolution of the PET images.[70]

PET imaging provides information with high contrast resolution, but is limited as a stand alone imaging modality due to its relatively low anatomical resolution.[64] However, the combination of PET and CT into a clinical hybrid PET/CT scanner enabled simultaneous functional and structural imaging. Additionally, information from the CT scan could now be used for attenuation correction of the PET images. This provided correct quantification of tracer uptake in each voxel. Another option which is recently introduced is the combination of PET and MRI, but this will not be further outlined here.

The introduction of a faster lutetium oxy-orthosilicate (LSO) scintillator ten years ago, with high light output, improved the spatial resolution from around 6.5 to 4 mm. This also brought down the possible image acquisition times to 5 minutes for a whole-body scan.[72] The LSO technology has further enabled time-of flight (TOF) scanners, which track the time difference between the two annihilation photons and thus improves the resolution and signal-to noise ratio.

As for CT and MRI, dynamic data acquisition is possible also for PET. This is performed by the use of list mode (LM) acquisition where all events are registered chronologically together with time stamps from the time of tracer injection. The

resulting dynamic image series thus include both the wash-in, or perfusion, phase and the metabolic phase. After completion of the image acquisition, data from a certain time interval can be selected and image reconstruction over that time interval may be performed. This allows for 4-D imaging of the temporal and spatial uptake of the tracer. As the tracer is distributed via the vascular network, dynamic PET (D-PET) can provide measures of tumour vasculature in addition to the active tracer uptake in target cells.

PET tracers

There is a large number of tracers available for PET imaging and a selection relevant for marking of metabolism, hypoxia and proliferation will be presented.[73]

The most widely used and investigated PET tracer is the glucose analogue FDG, which utilises the highly increased glucose metabolism in cancer cells.[64, 73] FDG is taken up by cells and phosphorylated by hexokinase to FDG-6-PO_4 (Fig. 5). Unlike the normal metabolite glucose-6-PO_4, this phosphate can not proceed in the glycolysis and is not further metabolised. FDG-6-PO_4 therefore accumulates in the cells and allows imaging of disease involvement.[74] A similar principle exists also for some of the other radiotracers described below. FDG uptake in the tumour is linked to aggressiveness, resistance to treatment and poor prognosis.[64, 75] Still, FDG is not an absolutely specific measure for tumour tissue. Other types of tissue also take up FDG, such as inflammatory tissue, salivary glands and certain muscles.

The upregulation of the glucose transporters (GLUTs) and the glycolytic hexokinase enzyme (HK-II) in the glycolytic pathway may be induced by the hypoxia-inducible factor (HIF-1α). It has therefore been discussed if FDG could serve also as a hypoxia marker.[76, 77] However, tumour cells can undergo glycolysis followed by anaerobic lactic acid fermentation even under aerobic conditions, called the Warburg effect.[78] It has been shown that FDG is not well suited for assessment of the oxygen status of tumours.[64, 77, 79]

Several PET tracers are available for imaging of hypoxia, predominantly for marking of chronic hypoxia.[19, 64] These are mainly 2-nitroimidazole derivates, such as ^{18}F-fluoromisonidazole (FMISO) and ^{18}F-azomycin-arabinoside (FAZA), which accumulate in hypoxic regions by binding to intracellular macromolecules in viable cells at low oxygen tensions. ^{64}Cu-methyl-thiosemicarbazone (^{64}Cu-ATSM) also

specifically accumulates in a hypoxic microenvironment, through the selective reduction of its metal component. Other hypoxia tracers are fluoroerythronitroimidazole (FETNIM), fluoroetanidazole (FETA) and the nitroimidazole EF5.[73]

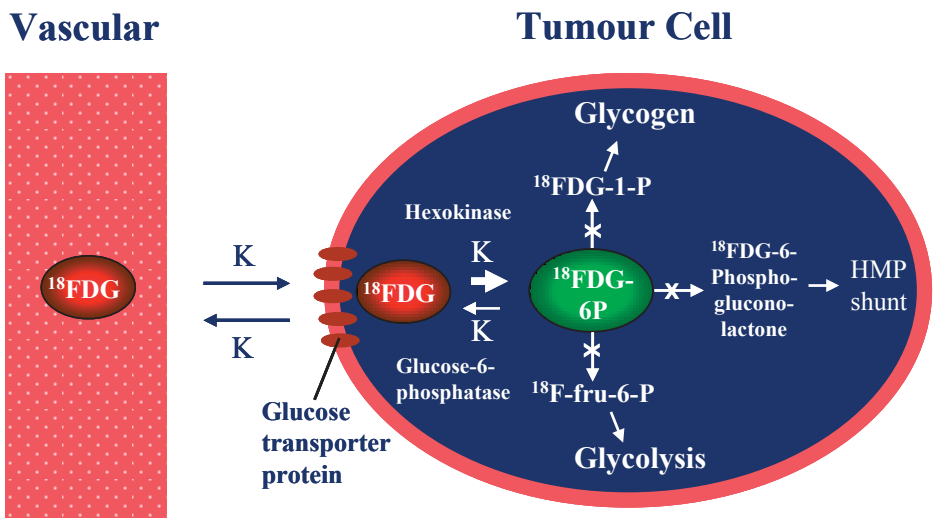

Figure 5. *The uptake and accumulation of FDG in cells. Adapted from Heron* et al.[74]

Tumour-cell proliferation can be successfully imaged using ^{18}F-fluorothymidine (FLT), which is retained inside the cell. FLT is specifically active during DNA synthesis and serves as S-phase marker. FLT PET may thus potentially be used to aid the identification of rapidly proliferating tumour subvolumes, and to prospectively assess the response to treatment.[64] Other proliferation radiotracers are also available, such as thymidine, deoxyuridine, methyl-methionine (MET) fluoroethyl-L-thyrosine (FET) and choline.[73]

All the factors causing increased radioresistance or recurrence of tumour growth should be included when defining the target volume for radiotherapy. The anatomically defined gross target volume (GTV) from CT and MRI should therefore preferably be expanded with a biological target volume (BTV), defined by specific radiotracers in PET. This may result in an expanded, reduced or spatially shifted GTV.[73]

SUV

The standardised uptake value (SUV) is used as a tool, both to supplement visual interpretation of tracer uptake in PET images and for semi-quantitative analysis. SUV is a dimensionless ratio of

$$SUV = \frac{Q_{tissue}}{Q_{normalizing}} \tag{12}$$

where Q is defined as average activity per unit volume. A $Q_{normalizing}$ can be the whole body, the contralateral anatomical site, or an organ, for example liver or brain.[80]

The reason for the SUV's popularity has been the need for a reliable reproducible measure of uptake. This need stems from intrapatient comparisons during therapy monitoring, from interpatient comparisons in the diagnostic process, relating to degrees of pathology, and from comparisons of data between institutions.[80] The SUV is subject to errors, however, and criticism about the methodology has been made.[81] Factors like body composition, length of uptake period, plasma glucose and partial volume effects should be considered.

3.6. Radiotherapy

Historical overview

Wilhelm Conrad Röntgen discovered x-rays in 1895 and the first treatment of cancer was accomplished less than 60 days later by Emil Grubbé in Chicago.[35] He initiated clinical radiotherapy by treating an advanced, ulcerated breast cancer in January 1896. However, treatments with these low-energy x-rays of 10-50 kV, and later with ortho-voltage x-rays of 200-500 kV, suffered from several drawbacks. The therapy had low penetration power, gave high surface layer doses in healthy tissue, and resulted in unwanted high doses in bone. Meanwhile, the discovery of natural radioactivity by Henry Becquerel in 1896 and isolation of radium in 1898 by Marie Curie paved the way for utilisation of high-energy photons in cancer therapy. Lead-encapsulated radium

needles and tubes were applied with a few centimetres of skin distance, and they enabled treatments of more deeply seated tumours. Other applications of radium were also developed, such as implantation of radium needles directly into the tumours, and irradiation via natural body cavities. Such brachytherapy applications are today still highly used, but now with sophisticated after loading equipment and a variety of radioactive isotopes as radiation sources.

Parallel to the development of radium therapy, new methods for producing high-energy radiation were developed. A method for accelerating electrons by means of radiofrequency fields was proposed by Gustaf Ising in 1925, and a real life model of a 50 keV linear accelerator (linac) was demonstrated by Rolf Widerøe four years later.[82] Before and during the Second World War, the microwave technology was developed and betatrons and higher energy electron linacs could thus be constructed. The first electron linac designed for radiotherapy was introduced at Hammersmith Hospital in London in 1953, and three years later there were seven clinical linacs altogether, worldwide.[82, 83] These high energy treatment beams overcame to a great extent the limitations of the low-energy and ortho-voltage x-rays.

During the last four decades technological progress has led to a significant improvement of the local control rates of many tumours, even in patients with locally advanced tumours.[35] Treatment planning and medical imaging has profited enormously from the revolution in computer technology. The functional and anatomical tissue properties mapped by CT, MRI and PET have enabled determination of the size and location of the tumour. Beam shaping and radiation shielding by MLCs in combination with advanced, intensity modulated beam delivery have further improved the possibility to maximise the dose to the tumour and minimise the dose to healthy normal tissue. Image guidance in radiotherapy has also contributed to this, and has enabled treatment monitoring and interactive adaptation of the treatment based on daily assessment of changes in tumour volume and response.[84]

The conventional linac gantry has an isocentric movement and rotates 360° around the patient (Fig. 6). The actual beam producing structure has not changed much over time, however, and the same technological principles are used today as in the time of early linac history. The later developments in treatment techniques have resulted mainly from the digitalisation of the linac control systems and from added equipment.

The last decade has also provided alternatives to the conventional x-ray linac design, such as the ring concepts of tomotherapy and of Vero, but these will not be outlined here. The utilisation of protons and heavy ions in cancer therapy will likewise not be described.

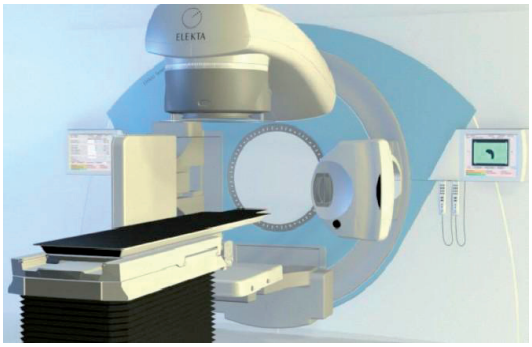

Figure 6. *Modern linear accelerator with add-on imaging equipment. Radiation gantry and collimator (above the table), volume imaging system x-ray source (to the right) and detector (to the left), and electronic portal imaging detector (below the table, partly covered). From Elekta AB web pages.*

Image registration and fusion

CT images are the foundation for 3-D dose planning. The planning CT may assume the role of an anatomically correct backdrop for the information provided by the MRI and PET modalities, which may have inherent image nonlinearity (MRI) or lack of anatomical resolution (PET).[85] Information from the two latter modalities may be included by manually comparison and hand transfer of the data to the planning CT, which is time consuming and unlikely to be accurate. The image sets can alternatively be fused by a full 3-D image registration. Such image registration is based mainly on two methods; landmark registration and intensity-based registration, the latter also called maximisation of mutual information.[67, 85]

Landmark registration is based on manual segmentation or identification of common structures in the two images to be aligned, and is suitable for image sets with clearly identifiable anatomical reference points, or markers. The intensity-based registration approach is an automatic iteration method. It utilises mutual information in

two images to find a similarity measure, which is maximised at the optimal alignment. Mutual information is user independent and suitable for images from different modalities. The integration of PET and CT into a dual-mode scanner has eliminated user-based registration for this modality. There are still pitfalls, however, since the two data sets are not acquired simultaneously and with different longitudinal table positions.[85]

When image registration has been performed, the image sets must be displayed in a coherent way to evaluate the relationship between them. A common way is to display the information from both images simultaneously as overlays in one image. Different methods for this are used, including colour overlay, dynamic alternating display, split view and subtracting images (Fig. 7).[67]

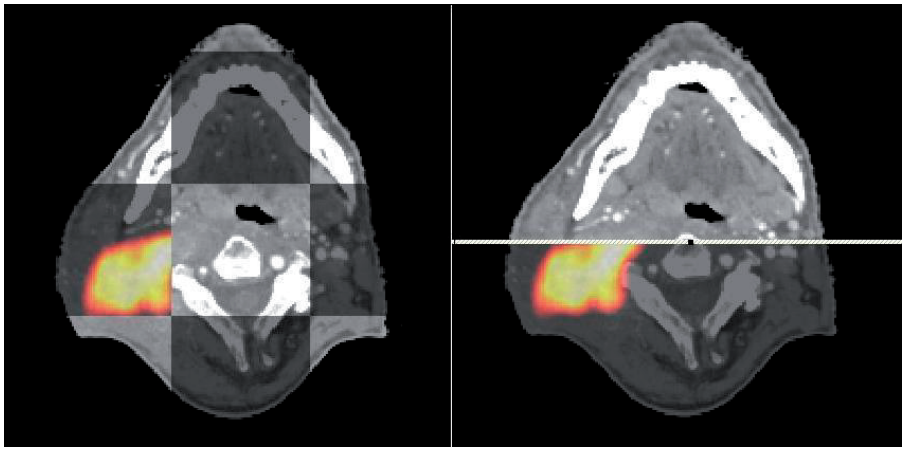

Figure 7. *CT image with colour PET overlay. Two types of split views are shown.*

IMRT

Intensity-modulated radiotherapy (IMRT) allows for the radiation dose to conform more precisely to the 3-D shape of the tumour compared to classical 3-D conformal radiotherapy (3-D CRT).[86, 87] IMRT provides the ability to deliver a high dose to the target volume, and at the same time spare normal tissues and critical structures that are

partially or fully surrounded by the target, or by a combination of targets (Fig. 8). IMRT also allows higher radiation doses to be delivered to regions within the tumour.

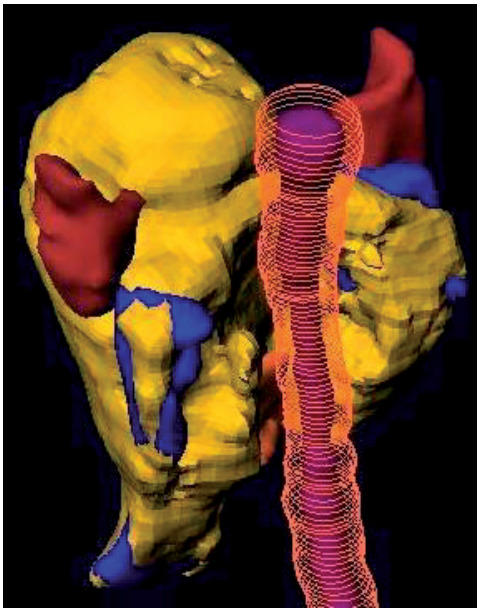

Figure 8. *Left posterior view of a head and neck cancer treated with IMRT. The 54 Gy isodose (dark yellow) is partly covering the planning target volume (PTV) (blue). The isodose surface is wrapped around the spinal cord (purple with orange margin) and the larynx (orange). The right and left parotids (brown) are partly spared.*

Advanced MLCs were on a broad scale released to the marked in the middle of the 1980s. These collimators had leaves of typically 10 mm width, which could be moved independently of each other into the treatment field. This facilitated both a more conformal shape of the treatment field and modulation of the photon beam intensity. IMRT, which was developed a few years earlier, could now be accomplished by modulating the intensity of a large number of small beamlets, typically 10x10 mm, within the radiation fields.[35, 88]

To determine the beamlet weights which achieved, or at least closely approximated, the desired dose distribution, inverse treatment planning algorithms were developed. Solving the inverse treatment planning problem was based on works from the 1980s and is today the most common strategy for IMRT.[89, 90] In inverse treatment

planning algorithms the desired dose to targets and dose limits of critical structures are defined as a basis, and intensity-modulated beam arrangements are derived to acceptably meet these desired dose objectives.[87] This is in contrast to forward planning algorithms, which have the treatment beams as a starting point. Commonly, the iterative inverse planning process is driven by the minimisation of a composite objective function, formed by weighting together the dose volume objectives, while fulfilling the dose volume constraints for the critical structures in a better and better way along the optimisation process.[91] By using a sequencer, the beamlets may be grouped together in typically 50 fields or more to assure a more efficient and faster delivery of the treatment.

IMRT may be delivered in different ways, but the main distinction is made between static and dynamic delivery. If the MLC leaves move during beam delivery, the treatment is referred to as dynamic, or sliding window.[87] If the beam is turned off between each change of the collimator setting, the delivery is termed step-and-shoot. Typically 7-12 beam directions, or gantry angels, are used for implementing an IMRT plan.[88] The beam may also be on during rotation of the gantry. This modality is then called volumetric modulated arc therapy (VMAT). The term intensity modulated arc therapy (IMAT) is also used.

MLCs with leaf widths down to 1.6 mm have been developed to increase the resolution of the treatment field. Some of these MLC types are add-on equipment introducing smaller maximum field sizes, while others are standard, full field collimators.

Dose painting

As described in chapter 3.3, radioresistance may be heterogeneously distributed within the tumour. The radioresistant regions may be targeted by integrating biological information into the inverse planning of IMRT. Different studies have suggested that molecular and functional imaging could form the basis for selective boosting of tumour subvolumes.[6, 8, 85, 92, 93] This procedure is called dose painting and strives to tailor the exact dose distribution needed for eradication of all tumour cells.[6, 7, 73, 88, 94] The benefit of this approach was shown by mathematical modelling more than 20 years ago, and later modelling studies of the dose painting concept have estimated large gains in

tumour control probabilities and improvements in dose distributions within the tumour volume.[9-14]

Planning for dose painting starts with segmentation of target volumes and organs at risk. These definitions are made on bases of CT images in combination with functional imaging, depicting biological processes in the tumour tissue that influence radiosensitivity (Fig. 9). Such imaging modalities may be PET, DCE-MRI, DCE-CT, and MRI spectroscopy.[7] Two different dose painting approaches have been proposed. Dose painting by contours (DPBC) prescribes a global dose objective inside the biological image-based contours, where the intention is to reach a certain dose value within the given target.[6, 8] Dose painting by numbers (DPBN), or dose painting by voxel intensity, prescribes the dose inside the target for each voxel as a function of the signal intensity of that voxel in the biological image (Fig. 10).[7, 9]

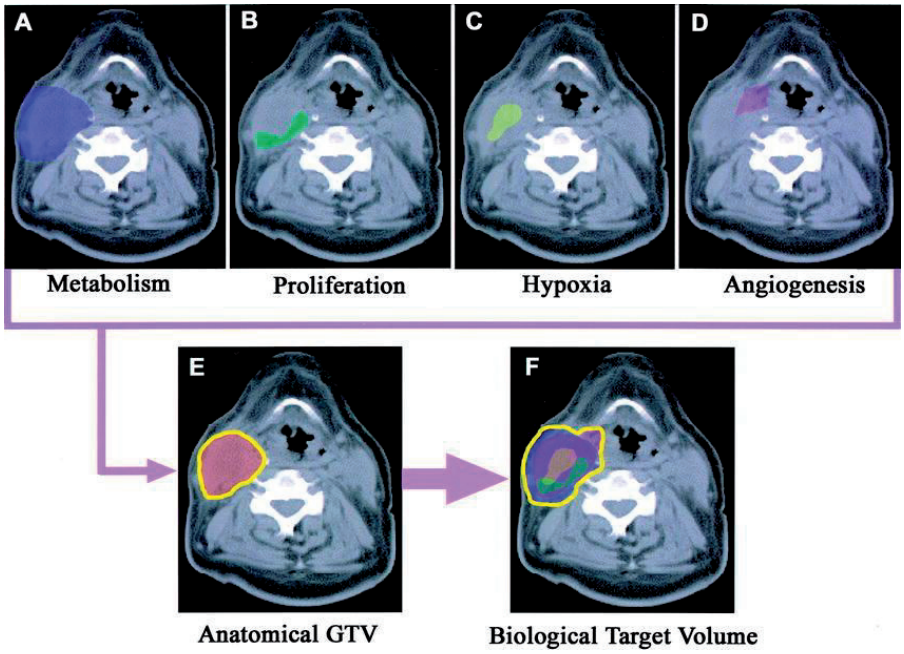

Figure 9. *Imaging paradigm in radiation oncology integrating different functional imaging modalities (panel A-D) with CT defined GTV (panel E) to obtain a combined BTV (panel F).*[73]

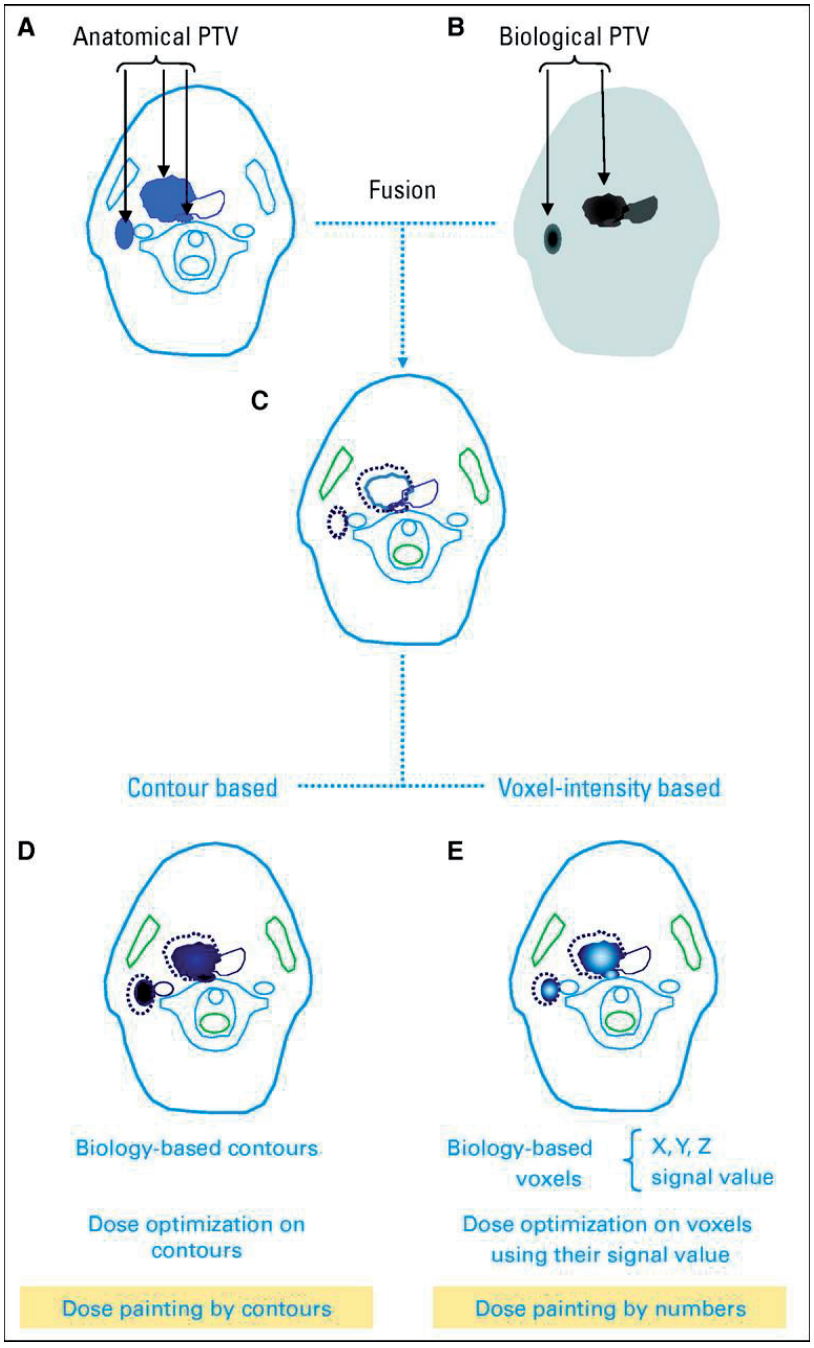

Figure 10. *(A) Anatomical PTV. (B) Biological PTV. (C) Fusion of (A) and (B). (D) contour based dose painting. (E) voxel-intensity based dose painting.*[88]

The dose prescriptions in dose painting are also differentiated in two strategies; dose escalation and dose redistribution. Dose escalation applies additional dose to the radioresistant subvolumes of the tumour.[95, 96] Dose redistribution increases the dose to the radioresistant parts while reducing the dose to the rest of the tumour, keeping the mean dose constant.[95-97]

Commercial treatment planning systems generally use dose-volume parameters to prescribe the desired dose distribution. This is not compatible with the DPBN approach, which uses voxel-based dose optimisation, and research treatment planning software has so far been a prerequisite for true DPBN planning.[98-100] However, the DPBC formalism may approach the DPBN formalism by increasing the number of contour levels.[21, 98] This makes planning for simplified DPBN feasible using an ordinary dose planning system, yet making optimisation and evaluation cumbersome as the number of volumes increases. In any case, a relationship between the biologically based voxel intensities and prescribed doses has to be established.[98, 99]

An inherent limitation in the resolution of the delivered dose distribution is caused by the application of photons as radiation source. The lateral scattering range and accompanying energy deposition several millimetres away from the interaction point inevitably restricts the obtainable steepness of the dose gradients.

The clinical value of dose painting has not yet been proven by appropriate trials.[88, 101] A few focal dose escalation studies have shown, however, that the treatments are well tolerated and do not increase normal tissue toxicity.[102, 103] There are a number of uncertainties and unknown factors which reside mainly in insufficient knowledge regarding the biological meaning of functional imaging, the predictive value of a given imaging parameter for radioresistance, and the uncertainties in the transformation of radiobiological factors to desired dose and dose constraints.[88, 98, 104] Another issue which have received little attention so far, is how well the treatment planning systems can deliver appropriate dose plans for dose painting objectives and the accuracy of such treatment deliveries.[21]

Due to the large dose gradients arising when prescribing focal dose escalation, one may further expect that high resolution MLCs will be a prerequisite. This is an issue which has received little attention in the literature so far.[21] MLC leaf width may be an

issue for effective treatment delivery in biologically adapted therapy and the problem should now be addressed.

In-room imaging systems

Developments in medical imaging have increased the ability to localise the target for precise administration of radiation. This is advantageous not only for designing treatment plans, but also for localisation of the target, the target motion, and the target changes during treatment. During the last decade the development within in-room imaging has moved from electronic portal imaging devices (EPIDs) towards volumetric patient imaging. For conventional linac designs, excluding tomotherapy and Vero, there are currently two main solutions for this; in-room CT, or CT-on-rails, and cone-beam CT.[105]

In-room CT is an integration of a CT-scanner in the linac treatment room, enabling imaging of diagnostic quality with the patient positioned on the treatment table. Imaging and treatment isocentres are not coincident, however, and the patient has to be transported on the treatment table between the two modalities.

CBCT systems perform tomographic reconstruction from a series of two-dimensional (planar) radiographs obtained by one half or one full rotation of the x-ray source around the patient. Due to the use of a cone-shaped beam and a large area flat panel detector, the whole longitudinal imaging volume of the patient is registered simultaneously (Fig. 11). This eliminates the need for a longitudinal movement of the patient during imaging. The image resolution is good, but the elevated levels of scattered radiation into the imaging system cause reduced image contrast compared to conventional CT systems.

Two main systems are in use for CBCT imaging. Kilovoltage (kV) cone-beam systems use a conventional CT x-ray generator as radiation source. This add-on system operates at a 90° angle with the treatment beam and introduces thereby sub optimal mechanical precision. Megavoltage (MV) cone-beam systems use the treatment beam for imaging. The imaging system is then in-line with the treatment system and has in principle identical isocentres. Artefacts from structures of high atomic number in the patient are avoided due to the high energy, and the images can in principle also be used for reconstruction of delivered doses. However, the MV beam energy causes low image

contrast compared with kV imaging and this may bring along higher radiation doses to obtain acceptable image quality.

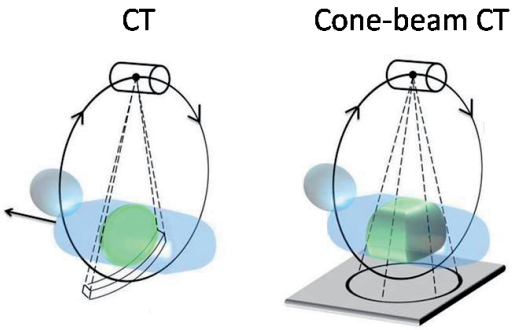

Figure 11. (*Left) Fan-shaped, conventional CT. (Right) CBCT.*

The reduced soft tissue contrast in the CBCT images hinders the utilisation of this application for biologically adapted therapy. Soft tissue tumours may not be visualised and this prevents tumour based image guiding and treatment monitoring. Improved tumour visibility would thus give benefits with regard to setup accuracy and tracking of target changes during treatment.

4. Methods and design

This section describes briefly some aspects of the experimental procedures applied in the present work. More detailed descriptions and literature references can be found in the original papers.

4.1. Canine patients, imaging and treatment

Paper I-III include PET/CT imaging and radiotherapy of three canine patients. These patients were companion dogs with naturally occurring head and neck cancers and the treatments were performed with curative intent. A brief summary of the patients and tumour characteristics is given in Table I. None of the dogs showed evidence of distant metastases at the time of diagnosis. The patients were included in a study approved by the Norwegian Animal Research Authority (NARA), and written informed consents were obtained from the owners.

Table I. *Canine patients included in the study*.

Patient ID	Patient breed	Gender*	Weight [kg]	Tumour location	Tumour histology	Initial tumour volume [cm^3]	Paper
A	Border collie	F	24	Right maxilla	Plasma cell tumour	14	I, II, III
B	Norwegian buhund	F	16	Right nasal cavity	Adeno-carcinoma	25	I
C	German shepherd	M	36	Left maxilla	Fibrosarcoma	65	I

* F: intact female, M: intact male

The patients were all given IMRT in treatment series of 10 fractions, one fraction a day. At five out of these treatments, CE-CBCT was performed (Fig. 12).

Dynamic and static PET/CT imaging was further performed before, during, and after the treatment series, and DCE-CT was performed before and after the treatment series.

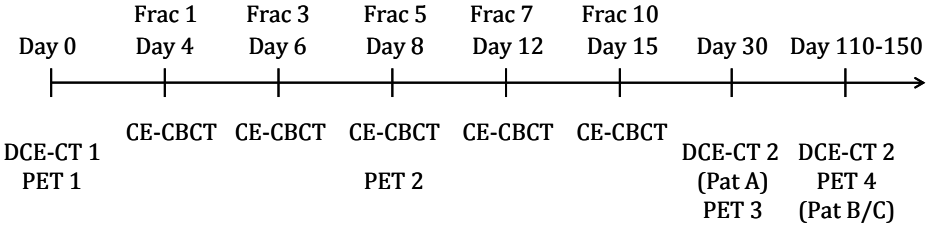

Figure 12. *Treatment and imaging schedule for the three canine patients. Day labels are indicative only, since there were variations between the patients. PET labels include dynamic and static PET.*

The three patients were given five fields IMRT with 6 MV photon energy. The treatments were planned using the Siemens VSIM virtual simulator (v 2.2) and KonRad inverse planning model (v 2.2.18) for patient A and B, and Nucletron Oncentra Masterplan (v 3.3) for patient C. The mean fraction dose to the GTV was 4.6 Gy for patient A and 4.7 Gy for patients B and C. The treatment machine was an Elekta Synergy linear accelerator, equipped with an XVI CBCT system. The dogs were placed in prone position on a vacuum cushion in a polymethyl methacrylate (PMMA) case. The upper jaws were fixed by a dental form to the PMMA case.

CE-CBCT imaging were performed prior to the IMRT at the sessions indicated (Fig. 12). The metabolic tumour status was monitored by dynamic and static PET imaging at day zero, which took place four days before the first treatment. Further PET sessions were set at fraction five of the IMRT and around two weeks after the last fraction. For patient B and C, a follow up PET examination was performed 3-4 months after the treatment. For patient A this PET scan was not implemented due to medical complications of the patient. DCE-CT was performed together with the PET imaging at the sessions before and after the treatment series.

PET/CT and DCE-CT imaging was done at a Siemens Biograph 16 scanner. Briefly, the imaging procedure started with administration of FDG with an activity of 6 MBq/kg, using a manual syringe. The scan duration for D-PET imaging was 45

minutes. Subsequently, when DCE-CT was included, 10 minutes of DCE-CT imaging was performed with the administration of 600-640 mg/kg Omnipaque (iohexol) for patient A and 600-640 mg/kg Visipaque (iodixanol) for patient B and C, at a concentration of 300 mg/ml. The imaging sessions were concluded with a whole body PET/CT, with an acquisition time of three minutes per bed.

Imaging and treatments were performed under general anaesthesia. At fraction five, the PET examination was done prior to the treatment session, with the patients kept continuously sedated till the end of the IMRT. DCE-CT was not performed at this session due to the possible toxic renal effects from the contrast agent.

4.2. The heterogeneous tumour model

The studies in paper IV and V utilised a previously established tumour model, based on a female canine patient with a spontaneous osteosarcoma in the nasal region. The gross target volume (GTV) was outlined in Gd-DTPA contrast-enhanced MR images. Uptake of tracer in the tumour tissue depends on blood flow, vascular density and extra vascular space. It has been suggested that these parameters may be related to hypoxia, and the MR tracer concentration thus served as a tentative marker for the partial pressure of oxygen.[51] The tumour was segmented into four compartments based on the tissue contrast concentration, and the compartments were in this way related to varying degrees of hypoxia. Due to the variation in vascularisation and distribution of tracer throughout the tumour, the four tumour compartments appeared highly heterogeneous and were partly split up into minor subvolumes. The model therefore represented an advanced and highly challenging prescription basis for IMRT.

IMRT planning

In paper IV the IMRT planning was done using the VSIM and KonRad systems. The MR images containing the compartmental information had previously been converted to CT DICOM standard and scaled to have a water-like composition with CT numbers around zero. The images were imported to the VSIM virtual simulator and the four compartments of the tumour model were defined by a manual contouring procedure in the VSIM module. For the IMRT planning, three different types of MLCs were

available, with leaf widths of 2.5, 5, and 10 mm. These MLCs represented real, commercially available hardware solutions.

In paper V another MLC was used. This was a BrainLab m3 micro MLC with 3.0 mm leaf width in the central part of the field, and 4.5 and 5.5 mm leafs laterally. A dedicated BrainLab iPlan Dose treatment planning system (v 3.0.2) was used for IMRT planning. The MLC is physically installed at one of our linacs, being in clinical use for stereotactic treatments.

5. Summary of results

5.1. Paper I

This paper investigated the resemblance in early tumour uptake patterns of a CT contrast agent and FDG PET tracer for three dogs with spontaneous head and neck tumours. DCE-CT and D-PET imaging were performed at two sessions. The first session was carried out four days before start of the fractionated radiotherapy. The second session was performed two weeks after end of treatment for patient A, four months after for patient B, and three months after for patient C (Fig. 12). Software tools were developed for downsampling the CT image series to the PET image dimensions, for segmentation of tracer uptake pattern in the tumours and for spatiotemporal correlation analysis of the images.

The analysis showed that DCE-CT images taken one minute post injection qualitatively resembled the D-PET images at all sessions, with the possible exception of session two for patient C where little uptake was seen in either image. Segmentation by region growing gave similar tumour extension in both modalities and a relatively high correlation was found between temporal uptake patterns from DCE-CT and D-PET. The heterogeneity in tumour uptake was not significantly different for the two modalities.

One could therefore conclude that early uptake patterns in tumours assessed by DCE-CT and D-PET gave similar results. Using D-PET alone for assessing both tumour perfusion and metabolic activity may thus be considered.

5.2. Paper II

This paper describes a feasibility study of a canine patient where the goal was to utilise contrast enhancement to visualise a soft tissue tumour on CBCT images. At five out of 10 fractions of IMRT, CBCT imaging was performed before and after administration of an iodinated contrast agent. Axial CBCT images were reconstructed and the pre-contrast images were subtracted from the post-contrast images. The subtraction images were

then over-laid on the pre-contrast images to visualise the contrast enhancement in an anatomical reference frame. For comparison, the same procedure was performed on DCE-CT images obtained at the PET/CT scanner.

The procedure produced a clearly visualised tumour in the CE-CBCT images for all five treatment sessions. A significant increase in contrast enhancement of 5.2 HU per treatment fraction was found. Further, a comparison of overlays for CE-CBCT, DCE-CT and PET/CT showed that the tumour extent and orientation appeared similar in the respective images.

CE-CBCT imaging was thus shown to be feasible and may be useful for online/offline setup corrections. This may be utilised separately or in combination with bony anatomy co-registration. Monitoring biological and spatial changes of the tumour is facilitated, which enables tumour boosting based on CBCT images.

5.3. Paper III

Paper three assessed the therapeutic gain in using tumour co-registration in favour of bony anatomy co-registration for setup corrections. Patient setup corrections with CBCT imaging have traditionally been based on bony anatomy co-registration. These corrections should ideally, however, be based on tumour localisation since the spatial relationship between the tumour and bony anatomy may change over the course of treatment.

In this paper, CE-CBCT images from five out of ten treatments of a canine patient were used to delineate gross tumour volumes (GTVs) for the purpose of radiotherapy adaptation. IMRT dose plans were generated on the basis of these delineations and different adaptation strategies were explored. The study showed that fully adapted dose planning, based on each CE-CBCT image series, gave EUDs closest to the prescription dose and the highest TCP.

Two other adaptive strategies were investigated, where dose planning was based on images acquired at the first treatment session. Patient repositioning was here performed either by bony anatomy co-registration, or by co-registration of the contrast enhanced images for the two strategies, respectively. These strategies gave EUDs and

TCPs close, but inferior, to the first strategy. A fourth approach, with no treatment adaptation or patient reposition, was clearly inferior to the other strategies.

This study showed that treatment adaptation based on CE-CBCT imaging was feasible and may lead to improved treatment outcome. An even higher benefit is expected in cases with soft tissue tumours showing larger changes in tumour position relative to bone and greater deformation than in the present study, where the tumour was partly located in bone.

5.4. Paper IV

This study aimed at exploring hypoxia dose painting by varying MLC leaf widths and IMRT parameter settings. Three different MLC leaf widths of 2.5, 5, and 10 mm and four different field arrangements were used, each optimised with four different step-and-shoot intensity levels. The seven fields/seven intensity levels plan was studied in more detail than the others, representing a commonly used parameter configuration.

Reducing the leaf widths increased the total TCP for all field arrangements. The effect on the total tumour control was generally larger when reducing from 10 to 5 mm leaf widths compared to reducing from 5 to 2.5 mm. For the seven fields/seven intensity levels plan, the TCP increase was most pronounced for the most hypoxic compartments. Increasing the number of fields generally also increased the TCP, while there were only minor effects on TCP by increasing the intensity levels above five.

Introducing systematic and random setup errors for the seven fields/seven intensity levels plan reduced the total TCP. When the errors exceeded 5 mm there were no longer any differences between the MLC types. When exceeding 7 mm setup errors there were only small differences in TCP between the redistributed and uniform treatment plans.

The current study indicated that reduced leaf widths are required for highly heterogeneous, biologically adapted radiotherapy. To achieve increased probability of cure, however, accurate patient setup is a crucial factor.

5.5. Paper V

The purpose of this work was to evaluate the radiobiological effects of planned and delivered high resolution IMRT, using dosimetric and radiobiological measures. A previously established tumour model with highly heterogeneous oxygen distribution was used as a clinical basis, virtually integrated into an anthropomorphic phantom head. A micro MLC with 3 mm minimum leaf width was used and the dose distributions were measured with Kodak EDR2 films in two planes. The dose planning was based on the principle of dose redistribution and three treatments were given.

The planned dose distributions appeared qualitatively conformal to the prescription, but the dose plan compartmental EUD values showed large reductions compared to the prescription. The deviation increased with increasing degree of hypoxia, with a maximum EUD reduction of 34% for the most hypoxic compartment in the caudal plane. The films showed high relative spatial accordance with the dose plan, demonstrated by low γ values in the γ analyses. The absolute compartmental mean doses for the films were 4-11% lower than expected from the planning, possibly due to errors in dose plan output factors for the smallest leaf openings.

The dose volume based IMRT could therefore not produce an optimal dose distribution for the highly heterogeneous tumour presented. Still, the biologically adapted radiotherapy was delivered with high precision according to the dose plan.

6. Discussion

Radioresistance in solid tumours have been counteracted by altering the radiotherapy schemes into hyperfractionated and accelerated schedules, and by combining with chemotherapeutics. In the current project, however, another approach has been investigated, namely dose painting and tumour visualisation before and during radiotherapy. The results may be of relevance for the definition of target volumes and for the implementation of dose escalation in biologically adapted radiotherapy.

Increase in tumour control and reduction of normal tissue adverse effects are the primary goals in radiotherapy research. Crucial factors have been the evolution of diagnostic tools and treatment techniques, and the increased knowledge in radiobiology. The progress made in CT, MRI, and PET imaging has enabled assessment of radioresistant tumour regions, and the development of treatment modalities like IMRT and VMAT has facilitated dose painting delivery.

Dose painting strategies puts stringent demands on spatial accuracy, both in the definition of target volume, in the assessment of radioresistant regions and in the quality control of treatment delivery. The latter was addressed in our work regarding adaptive therapy based on CE-CBCT (paper III), in the investigations of the influence of MLC leaf widths on biologically adapted IMRT plans (paper IV), and in the dosimetric verification of such plans (paper V).

IGRT procedures are crucial to ensure spatially correct dose deposition, both for conventional radiotherapy and for dose painting. The feasibility study of CE-CBCT (paper II) showed a novel application of the CBCT modality, which may be included in IGRT procedures. Using CE-CBCT during therapy may also enable monitoring of functional and anatomical tumour changes. This allows for treatment scheme adjustments in accordance with the functional and anatomical changes of the tumour. However, quantifying such alterations presupposes assessment of the functional and biological tumour properties prior to treatment. This aspect was addressed in the current work (papers I and II), demonstrating overlapping information from DCE-CT and D-PET.

6.1. Comparison of DCE-CT and D-PET

DCE-CT and D-PET are modalities that can provide information about tumour biology. It is, however, unclear whether the same or complementary information is acquired by the two methods. The initial distribution phase of CT contrast agent and PET tracer in the tumour are in principle analogous processes. The study of the three canine patients in paper I indicated that D-PET provided much of the same information and may be an alternative to DCE-CT. Contrast-induced nephropathy (CIN), diabetes, reduced renal function, and old age are among the risk factors for injection of iodinated CT contrast agents, and D-PET may be preferable for patients with such risk factors. The reduction of radiation exposure of the patient may also be a motivation for using D-PET rather than DCE-CT. Another advantage of PET is the combined imaging of vasculature, perfusion, and functional processes like metabolism, proliferation and hypoxia in one single uptake session. This can be particularly important for assessment of radioresistance.

There are, however, some restrictions in using D-PET rather than DCE-CT for treatment planning. One such limitation is the reduced spatial resolution of PET images compared to CT images. High-resolution DCE-CT images have been shown to correlate with the spatial distribution of blood vessel density in mouse models, and the high image resolution in CT may thus be a prerequisite for optimal application of dose painting.[106] Further, the intra-tumour heterogeneity in the current project (paper I) was reduced two- to three-fold when the CT images were re-sampled to PET resolution level. Such a reduction may lead to loss of information of the true biological tumour variations. This can have consequences for treatment efficacy and for treatment outcome prediction. Further studies are needed where these issues are addressed.

Another disadvantage of the D-PET modality is the increased occupation time of the scanner, which will be doubled compared with ordinary PET examinations. An exception is the first time slot in the morning, where the scanner is normally left unused for about one hour due to the rest period after the first tracer injection. Using D-PET on a larger scale with numerous patients each day will therefore inevitably impact patient throughput of the scanner. Other costs, as for PET tracer and hardware, will also be higher for D-PET compared with DCE-CT

6.2. Tumour visualisation by CE-CBCT

Tumour visualisation with CE-CBCT may be attractive since CBCT is now an integrated and customary component of newer linear accelerators. The usefulness of CE-CBCT for biologically adapted radiotherapy depends, however, on how well the technique can be utilised for proper tumour visualisation. Tumours in certain anatomical sites are less separable from surrounding soft tissues in ordinary CBCT images, as shown for example in a recent study for 1-2 cm (T1c) breast tumours on pre-operative CT scans.[107] This was also the case for the canine patient examined in the current project (paper II). Comparing pre- and post-contrast images, the mean tumour contrast enhancement was between 80 and 140 HU. This was not enough for satisfactory tumour visualisations in the post-contrast images. However, the image subtraction technique presented in paper II demonstrated a distinct visualisation of the tumour and was shown to be a feasible approach. The same procedure has at a later stage been applied for two other canine patients with head and neck tumours (patients B and C in Fig. 13). The results were in accordance with the first patient (patient A). The image subtraction technique may therefore be a useful tool for visualisation in biologically adapted radiotherapy.

The subtraction technique has drawbacks, however, that might limit its applicability. Pixel differences in pre- and post-contrast images caused by statistical noise and patient movements between image acquisitions will be visible in the overlays. This may disturb interpretation of the images, even if these effects to a certain extent can be counteracted by applying smoothing filters and precise co-registering of pre- and post-contrast image sets. Further, the method has to be adapted to clinical settings by developing software which can be safely operated by the treatment personnel. Also, the image analysis information has to be interpreted and translated into correction actions. There are therefore some steps to be taken on the technical side to make this procedure applicable.

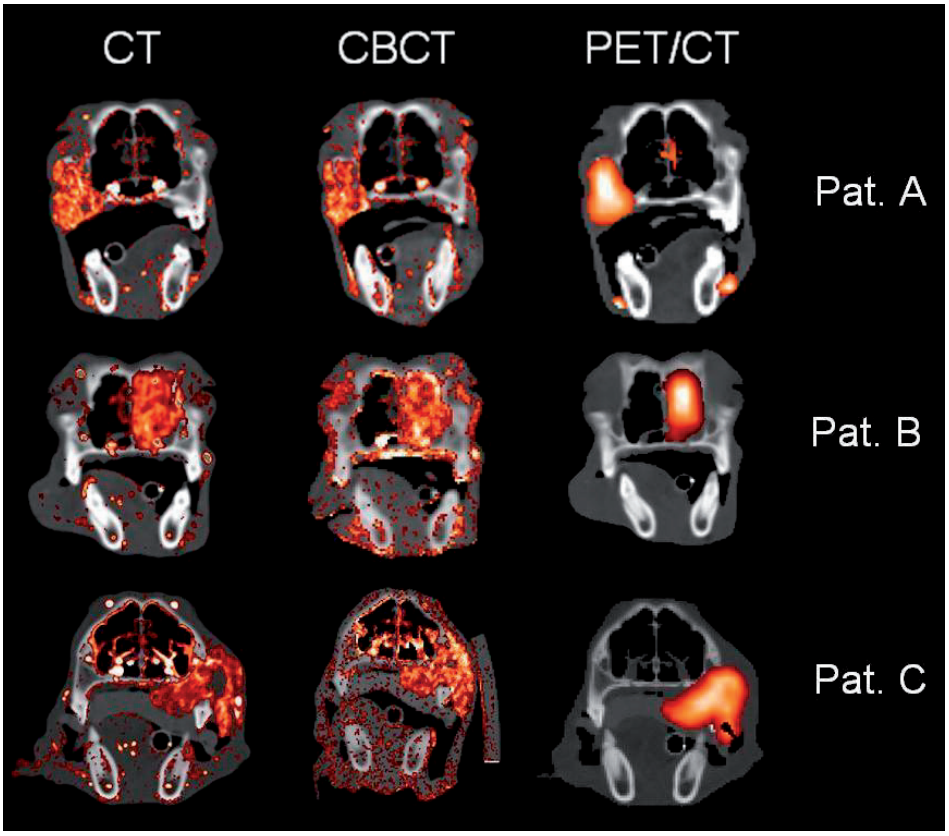

Figure 13. *The image subtraction and overlay technique applied on three canine patients, A, B, and C. (Left) CT overlay. (Middle) CBCT overlay. (Right) PET/CT overlay. Data presented at ESTRO29, at the 2nd Norwegian Conference in Medical Imaging and at CERRO 2011.*

6.3. Adaptive strategies

Adaptive treatment strategies based on tumour monitoring along the fractionated treatment course depend on reliable visualisation of the tumour and of the tumour changes caused by the therapy. For the case tested in paper III, the highest EUD values were obtained for fully adapted planning based on each of the five CE-CBCT image series. The advantage of such a strategy was assumed to be even larger for patients with more pronounced tumour positional changes relative to bone, and greater tumour

deformations during the treatment, than the case presented. Others have demonstrated large variation in the amount and rate of such positional changes and variations during radiotherapy, which had potential dosimetric impact when highly conformal treatment techniques were used.[108-110] By reliable visualisation of the tumour at the treatment unit, such tumour position variations and deformations could potentially be detected, and an optimal adaptive strategy could be pursued for each patient.

As outlined above, repeated CE-CBCT scans may not be appropriate for patients with certain risk factors related to injection of contrast agents. However, the use of nonionic contrast agents or novel, liposomal contrast agent formulations, co-encapsulating the iohexol molecule, may in near future allow frequent CE-CBCT imaging at a decreased risk of nephrotoxicity.[111] Development of such contrast agents may therefore prove to be beneficial also in radiotherapy settings.

6.4. Dose painting

Dose painting has been found technically feasible in several dose planning studies.[9, 96, 102, 103, 112-114] We are, however, aware of only four concluded dose painting trials; two FDG PET based trials on head and neck cancers and two MRI based dose escalation trials for prostate cancers.[102, 103, 115, 116] Trials for focal dose escalation of prostate cancer (FLAME) and FDG PET based lung cancer dose escalation are still accruing patients.[117, 118]

Both DPBN and level based DPBC have been found applicable, yet giving different results. While DPBC strives for a homogeneous dose within one or several defined contours, DPBN has the inherent ability of creating peak-dose regions according to the intensity variations of the voxels.[9] The intensity variation of the voxels in the dose prescription matrix depends on the resolution of the diagnostic images, however, and the realistically obtainable image resolution for PET images has up till now been 4-6 mm. Whether dose painting is applicable for prescription matrices of higher resolution, or for dose distributions with highly dispersed high dose areas, have to our knowledge not been closely investigated. Paper IV and V deal with these aspects in order to quantify the biological effects of such a high resolution, biologically adapted IMRT.

The dose painting principle in paper IV and V was contour based (DPBC), splitting the dose prescription matrix up into four dose levels. Still, the cases were approaching DPBN prescriptions, due to the dispersed nature of the four dose compartments. The voxel size of the dose prescription matrix was well below both what is obtainable with today's PET technology and also below obtainable accuracy in current, clinical target volume definitions. Paper IV showed that for this tumour model, reducing the MLC leaf widths from 10 down to 5 or 2.5 mm gave a considerable gain in biological effect, and high resolution MLCs may therefore be a prerequisite for focal treatment of such tumours. However, the advantage of small leaf widths diminished rapidly when spatial displacement errors were introduced. This was expected, since target volume margins were not applied in the dose planning. Today's clinical delineation and treatment accuracy may hence be of such a magnitude that the advantage of small leaf widths is reduced.

In paper V the planned and delivered IMRT was evaluated by radiobiological measures. Compared to the prescribed treatment, the results showed highly reduced mean doses and biological effect for the most hypoxic regions. Dispersed, small sized target volumes in combination with a considerable dose escalation, as investigated in the present work, may therefore not be properly dose painted with the current planning and treatment technology. Still, level based dose painting has been demonstrated to be successful with other boundary conditions.[21, 98] It is thus reasonable to assume that the spread and resolution of target subvolumes in the present tumour model, in addition to the large span in dose prescription levels, put restrictions on the treatment which the applied dose painting algorithm could not overcome. The limits for these constraints still remain to be determined.

It is further shown that DBDN with a biological optimisation objective gives higher peak doses for regions of high prescribed doses compared to the contour-based approach.[98, 100] Others have also demonstrated more successful dose painting with DPBN than DPBC.[96] One would therefore expect higher EUD values with the application of DPBN for the applied tumour model. However, such dose planning options are not yet available at our institution. The same considerations apply for alternative treatment techniques, like VMAT, which has successfully been evaluated in

combination with level based DPBC.[21] VMAT may thus be an option which should be considered for the given tumour model.

The true biological variations of radioresistance, which for hypoxia related radioresistance can appear within a few tenths of a millimetre, were not mapped with the present tumour model.[8] Dose adaptation to true radioresistance mapping is further far from being reached clinically, since the resolution in current PET imaging is even lower than for the applied tumour model. There are also issues on the treatment side, such as patient instability, treatment setup accuracy and dose gradient limitations of the IMRT, which put restrictions on the practical resolution of the resulting dose distribution. It has further been shown that the dose gradients in DPBN are reasonably congruent with the biological SUV gradients in current PET imaging.[98] True radioresistance dose adaptation may therefore not be desirable.[98] Still, the PET technology is evolving and TOF PET/CT scanning, giving better spatial resolution and improved visualisation of small uptake foci, is now possible.[119] Such progress thus contributes to further developments in dose painting.

7. Conclusions

This work revealed that assessment of early uptake patterns in tumours by D-PET and DCE-CT gave similar results for three canine patients studied. The contrast-enhancement technique developed was found to be feasible both for CBCT imaging and for conventional CT imaging and may be useful for online/offline setup corrections. Fully adapted dose planning based on each CE-CBCT image series gave a delivered treatment closest to the prescription. Reducing the MLC leaf widths may be beneficial for adapted radiotherapy. Reducing the leaf width from 10 to 5 mm gave higher estimated tumour effect than a reduction from 5 to 2.5 mm. Accurate patient setup is, however, a prerequisite for achieving increased probability of cure when using nonuniform instead of uniform dose distributions. IMRT of the heterogeneous tumour model produced a sub optimal dose distribution. Still, the treatments showed high relative spatial accordance with the dose plan.

8. Further perspectives

The present thesis is to a great extent based on case studies. Further research should therefore aim at including patients in clinical trials to test the validity of the results on a larger scale. Implementing CE-CBCT in a clinical setting is discussed above and presupposes a certain refinement of software applications for user-friendly handling of the procedures. Parallel to this it will be possible, however, to apply the technique on a simplified technical basis for head and neck radiotherapy patients undergoing PET/CT examinations. The CT part of these examinations is now routinely performed with iv contrast as the standard method. One additional CT pre-scan without contrast is therefore sufficient to supply data for the contrast enhancement technique developed. Such investigations will produce valuable image information from a CBCT-like clinical setting and can give indications whether the technique is of clinical relevance. Data from a pilot patient have been analysed and the results seem to be in line with the results from the canine treatment study (Fig. 14).

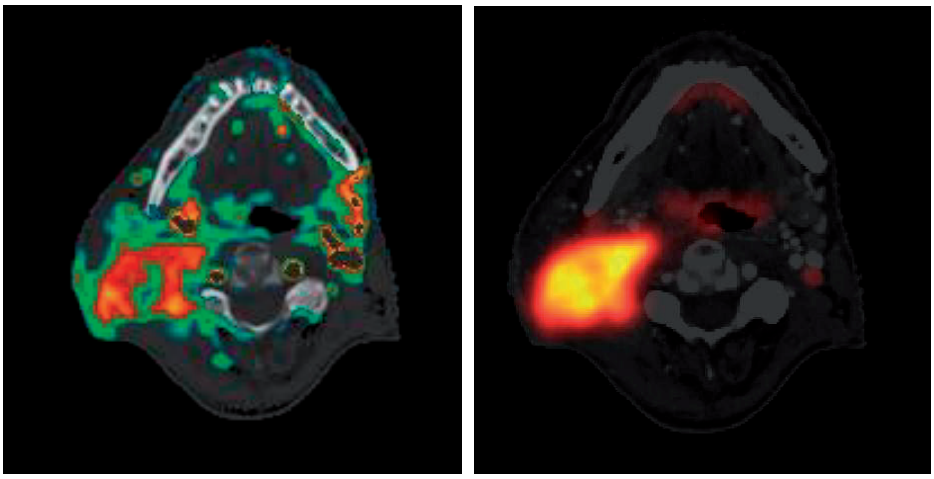

Figure 14. *(Left) The image subtraction and overlay technique applied on CE-CT images of a human head and neck patient. The contrast enhancement in large blood vessels is set to zero. (Right) FDG PET/CT image of the same patient.*

Numerous studies show a significant relation between high pre-therapy SUV_{max} and reduced disease-free survival for head and neck patients.[120] A relationship has further been shown between pre-treatment tumour vascular parameters, measured by DCE-MRI, and reduction in FDG metabolism after one cycle of chemotherapy for breast carcinoma patients.[121] Here, a well developed vascular network, as measured by DCE-MRI, gave more effective chemotherapy, with cell kill measured by FDG-PET. Later studies on maximum tolerated doses for head and neck treatments have shown that dose escalation is possible without introducing severe toxic effects in the patients.[99, 102] These studies motivate for a clinical trial for head and neck cancer patients comparing dose painting based on FDG PET imaging with conventional treatment. As chemotherapy is given concomitantly, monitoring of vascular status with DCE-CT before and during treatment may give valuable information with respect to identifying patients not responding to therapy. Furthermore, as DCE-CT vascular status also may be linked to hypoxia, this imaging modality could play a role in predicting radiation response. Alternatively, the combined DCE-CT and static PET examination may be replaced by a D-PET scan only. CE-CBCT, as discussed above, would also be possible within the limits set by kidney tolerance. Such studies represent a follow up of the techniques presented in the current work and may give information on the relation between dose escalation effects and metabolic and vascular parameters.

Treatment planning algorithms for VMAT will shortly be introduced at our hospital. This will give us the opportunity to repeat the dosimetric investigation of dose painting by the use of another treatment technique. Planning systems offering DPBN and biological optimisation objectives should also be searched for and tested, and studies involving such technology may be a future option.

Bibliography

1. Tredan O, Galmarini CM, Patel K*, et al.* Drug resistance and the solid tumor microenvironment. *Journal of the National Cancer Institute* 2007;99:1441-1454.
2. Vaupel P. Tumor microenvironmental physiology and its implications for radiation oncology. *Seminars in Radiation Oncology* 2004;14:198-206.
3. Laskar SG, Agarwal JP, Srinivas C*, et al.* Radiotherapeutic management of locally advanced head and neck cancer. *Expert Review of Anticancer Therapy* 2006;6:405-417.
4. Chao KSC, Ozyigit G, Tran BN*, et al.* Patterns of failure in patients receiving definitive and postoperative IMRT for head-and-neck cancer. *International Journal of Radiation Oncology Biology Physics* 2003;55:312-321.
5. Cellini N, Morganti AG, Mattiucci GC*, et al.* Analysis of intraprostatic failures in patients treated with hormonal therapy and radiotherapy: Implications for conformal therapy planning. *International Journal of Radiation Oncology Biology Physics* 2002;53:595-599.
6. Ling CC, Humm J, Larson S*, et al.* Towards multidimensional radiotherapy (MD-CRT): Biological imaging and biological conformality. *International Journal of Radiation Oncology Biology Physics* 2000;47:551-560.
7. Bentzen SM. Theragnostic imaging for radiation oncology: dose-painting by numbers. *Lancet Oncology* 2005;6:112-117.
8. Chao KSC, Bosch WR, Mutic S*, et al.* A novel approach to overcome hypoxic tumor resistance: Cu-ATSM-guided intensity-modulated radiation therapy. *International Journal of Radiation Oncology Biology Physics* 2001;49:1171-1182.
9. Vanderstraeten B, Duthoy W, De Gersem W*, et al.* [F-18]fluoro-deoxy-glucose positron emission tomography ([F-18]FDG-PET) voxel intensity-based intensity-modulated radiation therapy (IMRT) for head and neck cancer. *Radiotherapy and Oncology* 2006;79:249-258.
10. Sovik A, Malinen E, Bruland OS*, et al.* Optimization of tumour control probability in hypoxic tumours by radiation dose redistribution: a modelling study. *Physics in Medicine and Biology* 2007;52:499-513.
11. Stavreva NA, Stavrev PV, Round WH. A mathematical approach to optimizing the radiation dose distribution in heterogeneous tumours. *Acta Oncologica* 1996;35:727-732.
12. Brahme A, Agren AK. Optimal Dose Distribution for Eradication of Heterogeneous Tumors. *Acta Oncologica* 1987;26:377-385.
13. Brahme A. Biologically optimized 3-dimensional in vivo predictive assay-based radiation therapy using positron emission tomography-computerized tomography Imaging. *Acta Oncologica* 2003;42:123-136.
14. Popple RA, Ove R, Shen S. Tumor control probability for selective boosting of hypoxic subvolumes, including the effect of reoxygenation. *International Journal of Radiation Oncology Biology Physics* 2002;54:921-927.
15. Just what is Molecular Imaging?: Center for Molecular Imaging Innovation and Translation.

16. ClinicalTrials.gov. Functional Imaging of Tumor and Normal Tissue (FITT). 2011.
17. Glunde K, Pathak AP, Bhujwalla ZM. Molecular-functional imaging of cancer: to image and imagine. *Trends in Molecular Medicine* 2007;13:287-297.
18. Malinen E. Spatiotemporal analysis of tumor uptake patterns in dynamic 18FDG-PET and dynamic contrast enhanced CT. 2011.
19. Sovik A, Malinen E, Olsen DR. Strategies for Biologic Image-Guided Dose Escalation: a Review. *International Journal of Radiation Oncology Biology Physics* 2009;73:650-658.
20. Thorwarth D, Alber M. Implementation of hypoxia imaging into treatment planning and delivery. *Radiotherapy and Oncology* 2010;97:172-175.
21. Korreman SS, Ulrich S, Bowen S*, et al.* Feasibility of dose painting using volumetric modulated arc optimization and delivery. *Acta Oncologica* 2010;49:964-971.
22. U.S. National Institutes of Health, National Cancer Institute (www.cancer.gov).
23. Brown JM. Exploiting the hypoxic cancer cell: mechanisms and therapeutic strategies. *Molecular Medicine Today* 2000;6:157-162.
24. Sporn MB. The war on cancer. *Lancet* 1996;347:1377-1381.
25. Hanahan D, Weinberg RA. The hallmarks of cancer. *Cell* 2000;100:57-70.
26. Hanahan D, Weinberg RA. Hallmarks of Cancer: The Next Generation. *Cell* 2011;144:646-674.
27. American Cancer Sosiety Inc. (www.cancer.org).
28. Radiotherapy in Norway: Norwegian Radiation Protection Authority; 2010.
29. Cancer in Norway 2009: Cancer Registry of Norway, Institute of population-based cancer research; 2011.
30. Miles KA. Tumour angiogenesis and its relation to contrast enhancement on computed tomography: a review. *European Journal of Radiology* 1999;30:198-205.
31. Vaupel P. The role of hypoxia-induced factors in tumor progression. *Oncologist* 2004;9:10-17.
32. Vaupel P, Mayer A. Hypoxia and anemia: effects on tumor biology and treatment resistance. *Transfusion Clinique Et Biologique* 2005;12:5-10.
33. Wilson GD. Cell kinetics. *Clinical Oncology* 2007;19:370-384.
34. Paoloni M, Khanna C. Science and society - Translation of new cancer treatments from pet dogs to humans. *Nature Reviews Cancer* 2008;8:147-156.
35. Bernier J, Hall EJ, Giaccia A. Timeline - Radiation oncology: a century of achievements. *Nature Reviews Cancer* 2004;4:737-U715.
36. Gray LH, Conger AD, Ebert M*, et al.* The Concentration of Oxygen Dissolved in Tissues at the Time of Irradiation as a Factor in Radiotherapy. *British Journal of Radiology* 1953;26:638-648.
37. Steel GG. Basic Clinical Radiobiology. Third edition. *London: Hodder Arnold Publication* 2002.
38. Bourhis J, Overgaard J, Audry H*, et al.* Hyperfractionated or accelerated radiotherapy in head and neck cancer: a meta-analysis. *Lancet* 2006;368:843-854.
39. Bussink J, van der Kogel AJ, Kaanders J. Activation of the PI3-K/AKT pathway and implications for radioresistance mechanisms in head and neck cancer. *Lancet Oncology* 2008;9:288-296.

40. Dutreix M, Cosset JM, Sun JS. Molecular therapy in support to radiotherapy. *Mutation Research-Reviews in Mutation Research* 2010;704:182-189.
41. Harima Y, Sawada S, Miyazaki Y*, et al.* Expression of Ku80 in cervical cancer correlates with response to radiotherapy and survival. *Am J Clin Oncol* 2003;26:e80-85.
42. Santucci MA, Barbieri E, Frezza G*, et al.* Radiation-induced Gadd45 expression correlates with clinical response to radiotherapy of cervical carcinoma. *International Journal of Radiation Oncology Biology Physics* 2000;46:411-416.
43. Wilson CR, Davidson SE, Margison GP*, et al.* Expression of Ku70 correlates with survival in carcinoma of the cervix. *British Journal of Cancer* 2000;83:1702-1706.
44. Joiner M, van der Kogel A. Basic Clinical Radiobiology. Fourth edition. *Hodder Arnold* 2009.
45. West CML, Davidson SE, Roberts SA*, et al.* The independence of intrinsic radiosensitivity as a prognostic factor for patient response to radiotherapy of carcinoma of the cervix. *British Journal of Cancer* 1997;76:1184-1190.
46. Bjork-Eriksson T, West C, Karlsson E*, et al.* Tumor radiosensitivity (SF2) is a prognostic factor for local control in head and neck cancers. *International Journal of Radiation Oncology Biology Physics* 2000;46:13-19.
47. Forastiere AA, Goepfert H, Maor M*, et al.* Concurrent chemotherapy and radiotherapy for organ preservation in advanced laryngeal cancer. *New England Journal of Medicine* 2003;349:2091-2098.
48. Maciejewski B, Withers HR, Taylor JMG*, et al.* Dose Fractionation and Regeneration in Radiotherapy for Cancer of the Oral Cavity and Oropharynx - Tumor Dose-Response and Repopulation. *International Journal of Radiation Oncology Biology Physics* 1989;16:831-843.
49. Withers HR, Taylor JMG, Maciejewski B. The Hazard of Accelerated Tumor Clonogen Repopulation During Radiotherapy. *Acta Oncologica* 1988;27:131-146.
50. Kim JJ, Tannock IF. Repopulation of cancer cells during therapy: An important cause of treatment failure. *Nature Reviews Cancer* 2005;5:516-525.
51. Zahra MA, Hollingsworth KG, Sala E*, et al.* Dynamic contrast-enhanced MRI as a predictor of tumour response to radiotherapy. *Lancet Oncology* 2007;8:63-74.
52. Nordsmark M, Overgaard J. Tumor hypoxia is independent of hemoglobin and prognostic for loco-regional tumor control after primary radiotherapy in advanced head and neck cancer. *Acta Oncol* 2004;43:396-403.
53. Lyng H, Sundfor K, Trope C*, et al.* Disease control of uterine cervical cancer: relationships to tumor oxygen tension, vascular density, cell density, and frequency of mitosis and apoptosis measured before treatment and during radiotherapy. *Clin Cancer Res* 2000;6:1104-1112.
54. Overgaard J, Eriksen JG, Nordsmark M*, et al.* Plasma osteopontin, hypoxia, and response to the hypoxia sensitiser nimorazole in radiotherapy of head and neck cancer: results from the DAHANCA 5 randomised double-blind placebo-controlled trial. *Lancet Oncol* 2005;6:757-764.
55. Nahum AE, Sanchez-Nieto B. Tumour control probability modelling: Basic principles and applications in treatment planning. *Physica Medica* 2001;17:13-23.

56. Webb S, Nahum AE. A Model for Calculating Tumor-Control Probability in Radiotherapy Including the Effects of Inhomogeneous Distributions of Dose and Clonogenic Cell-Density. *Physics in Medicine and Biology* 1993;38:653-666.
57. Sanchez-Nieto B, Nahum AE. The delta-TCP concept: a clinically useful measure of tumor control probability. *Int J Radiat Oncol Biol Phys* 1999;44:369-380.
58. Sovik A, Ovrum J, Olsen DR*, et al.* On the parameter describing the generalised equivalent uniform dose (gEUD) for tumours. *Physica Medica* 2007;23:100-106.
59. Beckmann EC. CT scanning the early days. *British Journal of Radiology* 2006;79:5-8.
60. Mansfield P, Maudsley AA. Medical Imaging by Nmr. *British Journal of Radiology* 1977;50:188-194.
61. Terpogossian MM, Phelps ME, Hoffman EJ*, et al.* Positron-Emission Transaxial Tomograph for Nuclear Imaging (Pett). *Radiology* 1975;114:89-98.
62. Ido T, Wan CN, Casella V*, et al.* Labeled 2-Deoxy-D-Glucose Analogs - F-18-Labeled 2-Deoxy-2-Fluoro-D-Glucose, 2-Deoxy-2-Fluoro-D-Mannose and C-14-2-Deoxy-2-Fluoro-D-Glucose. *Journal of Labelled Compounds & Radiopharmaceuticals* 1978;14:175-183.
63. Townsend DW. Dual-modality imaging: Combining anatomy and function. *Journal of Nuclear Medicine* 2008;49:938-955.
64. Bussink J, Kaanders J, van der Graaf WTA*, et al.* PET-CT for radiotherapy treatment planning and response monitoring in solid tumors. *Nature Reviews Clinical Oncology* 2011;8:233-242.
65. Khan FM. The Physics of Radiation Therapy. 1984.
66. Knoos T, Nilsson M, Ahlgren L. A Method for Conversion of Hounsfield Number to Electron-Density and Prediction of Macroscopic Pair Production Cross-Sections. *Radiotherapy and Oncology* 1986;5:337-345.
67. Nucletron BV. Oncentra External Beam v4.0, Physics and algoritms.
68. Rogalla P, Kloeters C, Hein PA. CT Technology Overview: 64-Slice and Beyond. *Radiologic Clinics of North America* 2009;47:1-+.
69. Lee TY, Purdie TG, Stewart E. CT imaging of angiogenesis. *Quarterly Journal of Nuclear Medicine* 2003;47:171-187.
70. Dowsett DJ, Kenny PA, Johnston RE. The Physics of Diagnostic Imaging, Second edition. *Oxford University Press Inc., New York* 2006.
71. Cooper RA, Carrington BM, Loncasters JA*, et al.* Tumour oxygenation levels correlate with dynamic contrast-enhanced magnetic resonance imaging parameters in carcinoma of the cervix. *Radiotherapy and Oncology* 2000;57:53-59.
72. Patton JA, Townsend DW, Hutton BF. Hybrid Imaging Technology: From Dreams and Vision to Clinical Devices. *Seminars in Nuclear Medicine* 2009;39:247-263.
73. Apisarnthanarax S, Chao KSC. Current Imaging paradigms in radiation oncology. *Radiation Research* 2005;163:1-25.
74. Heron DE, Smith RP, Andrade RS. Advances in image-guided radiation therapy - The role of PET-CT. *Medical Dosimetry* 2006;31:3-11.

75. Mankoff DA, Eary JF, Link JM*, et al.* Tumor-specific positron emission tomography Imaging in patients: [F-18) fluorodeoxyglucose and beyond. *Clinical Cancer Research* 2007;13:3460-3469.
76. Pugachev A, Ruan S, Carlin S*, et al.* Dependence of FDG uptake on tumor microenvironment. *International Journal of Radiation Oncology Biology Physics* 2005;62:545-553.
77. Christian N, Deheneffe S, Bol A*, et al.* Is F-18-FDG a surrogate tracer to measure tumor hypoxia? Comparison with the hypoxic tracer C-14-EF3 in animal tumor models. *Radiotherapy and Oncology* 2010;97:183-188.
78. Warburg O. Respiratory Impairment in Cancer Cells. *Science* 1956;124:269-270.
79. Busk M, Horsman MR, Jakobsen S*, et al.* Cellular uptake of PET tracers of glucose metabolism and hypoxia and their linkage. *European Journal of Nuclear Medicine and Molecular Imaging* 2008;35:2294-2303.
80. Thie JA. Understanding the standardized uptake value, its methods, and implications for usage. *Journal of Nuclear Medicine* 2004;45:1431-1434.
81. Keyes JW. Suv - Standard Uptake or Silly Useless Value. *Journal of Nuclear Medicine* 1995;36:1836-1839.
82. Marton L, Marton C. Advances in electronics and electron physics. . *Academic Press, Inc.* 1980;50.
83. Thwaites DI, Tuohy JB. Back to the future: the history and development of the clinical linear accelerator. *Physics in Medicine and Biology* 2006;51:R343-R362.
84. Verellen D, De Ridder M, Storme G. A (short) history of image-guided radiotherapy. *Radiotherapy and Oncology* 2008;86:4-13.
85. Rosenman J. Incorporating functional imaging information into radiation treatment. *Seminars in Radiation Oncology* 2001;11:83-92.
86. www.radiologyinfo.org.
87. Galvin JM, Ezzell G, Eisbrauch A*, et al.* Implementing IMRT in clinical practice: A joint document of the American Society for Therapeutic Radiology and Oncology and the American Association of Physicists in Medicine. *International Journal of Radiation Oncology Biology Physics* 2004;58:1616-1634.
88. Galvin JM, De Neve W. Intensity modulating and other radiation therapy devices for dose painting. *Journal of Clinical Oncology* 2007;25:924-930.
89. Brahme A, Roos JE, Lax I. Solution of an Integral-Equation Encountered in Rotation Therapy. *Physics in Medicine and Biology* 1982;27:1221-1229.
90. Censor Y, Altschuler MD, Powlis WD. A Computational Solution of the Inverse Problem in Radiation-Therapy Treatment Planning. *Applied Mathematics and Computation* 1988;25:57-87.
91. Nucletron BV. Oncentra External Beam v4.0 User Manual. Ref 170.730.
92. Tome WA, Fowler JF. Selective boosting of tumor subvolumes. *International Journal of Radiation Oncology Biology Physics* 2000;48:593-599.
93. Chapman JD, Schneider RF, Urbain JL*, et al.* Single-photon emission computed tomography and positron-emission tomography assays for tissue oxygenation. *Seminars in Radiation Oncology* 2001;11:47-57.
94. Tanderup K, Olsen DR, Grau C. Dose painting: Art or science? *Radiotherapy and Oncology* 2006;79:245-248.

95. Alber M, Paulsen F, Eschmann SM, *et al.* On biologically conformal boost dose optimization. *Physics in Medicine and Biology* 2003;48:N31-N35.
96. Thorwarth D, Eschmann SM, Paulsen F, *et al.* Hypoxia dose painting by numbers: A planning study. *International Journal of Radiation Oncology Biology Physics* 2007;68:291-300.
97. Sovik A, Malinen E, Skogmo HK, *et al.* Radiotherapy adapted to spatial and temporal variability in tumor hypoxia. *International Journal of Radiation Oncology Biology Physics* 2007;68:1496-1504.
98. Meijer G, Steenhuijsen J, Bal M, *et al.* Dose painting by contours versus dose painting by numbers for stage II/III lung cancer: Practical implications of using a broad or sharp brush. *Radiother Oncol* 2011;100:396-401.
99. Madani I, Duprez F, Boterberg T, *et al.* Maximum tolerated dose in a phase I trial on adaptive dose painting by numbers for head and neck cancer. *Radiother Oncol* 2011;2011:8.
100. Vanderstraeten B, De Gersem W, Duthoy W, *et al.* Implementation of biologically conformal radiation therapy (BCRT) in an algorithmic segmentation-based inverse planning approach. *Physics in Medicine and Biology* 2006;51:N277-N286.
101. Pijls-Johannesma M, van Mastrigt G, Hahn SM, *et al.* A systematic methodology review of phase I radiation dose escalation trials. *Radiotherapy and Oncology* 2010;95:135-141.
102. Madani I, Duthoy W, Derie C, *et al.* Positron emission tomography-guided, focal-dose escalation using intensity-modulated radiotherapy for head and neck cancer. *International Journal of Radiation Oncology Biology Physics* 2007;68:126-135.
103. Duprez F, De Neve W, De Gersem W, *et al.* Adaptive Dose Painting by Numbers for Head-and-Neck Cancer. *International Journal of Radiation Oncology Biology Physics* 2011;80:1045-1055.
104. Busk M, Horsman MR, Overgaard J. Resolution in PET hypoxia imaging: Voxel size matters. *Acta Oncologica* 2008;47:1201-1210.
105. Dawson LA, Jaffray DA. Advances in image-guided radiation therapy. *Journal of Clinical Oncology* 2007;25:938-946.
106. Cao MS, Liang YR, Shen CY, *et al.* Developing DCE-CT to Quantify Intra-Tumor Heterogeneity in Breast Tumors With Differing Angiogenic Phenotype. *Ieee Transactions on Medical Imaging* 2009;28:861-871.
107. Boersma LJ, Hanbeukers B, Boetes C, *et al.* Is contrast enhancement required to visualize a known breast tumor in a pre-operative CT scan? *Radiotherapy and Oncology* 2011;100:271-275.
108. Knap MM, Hoffmann L, Nordsmark M, *et al.* Daily cone-beam computed tomography used to determine tumour shrinkage and localisation in lung cancer patients. *Acta Oncologica* 2010;49:1077-1084.
109. Barker JL, Garden AS, Ang KK, *et al.* Quantification of volumetric and geometric changes occurring during fractionated radiotherapy for head-and-neck cancer using an integrated CT/linear accelerator system. *International Journal of Radiation Oncology Biology Physics* 2004;59:960-970.
110. Geets X, Tomsej M, Lee JA, *et al.* Adaptive biological image-guided IMRT with anatomic and functional imaging in pharyngo-laryngeal tumors: Impact on

target volume delineation and dose distribution using helical tomotherapy. *Radiotherapy and Oncology* 2007;85:105-115.
111. Zheng JZ, Liu JB, Dunne M*, et al.* In vivo performance of a liposomal vascular contrast agent for CT and MR-based image guidance applications. *Pharmaceutical Research* 2007;24:1193-1201.
112. Thorwarth D, Geets X, Paiusco M. Physical radiotherapy treatment planning based on functional PET/CT data. *Radiotherapy and Oncology* 2010;96:317-324.
113. Korreman S, Medin J, Kjaer-Kristoffersen F. Dosimetric verification of RapidArc treatment delivery. *Acta Oncologica* 2009;48:185-191.
114. Schwartz DL, Ford EC, Rajendran J*, et al.* FDG-PET/CT-guided intensity modulated head and neck radiotherapy: A pilot investigation. *Head and Neck-Journal for the Sciences and Specialties of the Head and Neck* 2005;27:478-487.
115. Fonteyne V, Villeirs G, Speleers B*, et al.* Intensity-modulated radiotherapy as primary therapy for prostate cancer: Report on acute toxicity after dose escalation with simultaneous integrated boost to intraprostatic lesion. *International Journal of Radiation Oncology Biology Physics* 2008;72:799-807.
116. Singh AK, Guion P, Sears-Crouse N*, et al.* Simultaneous integrated boost of biopsy proven, MRI defined dominant intra-prostatic lesions to 95 Gray with IMRT: early results of a phase I NCI study. *Radiation Oncology* 2007;2.
117. ClinicalTrials.gov. FLAME: Investigate the Benefit of a Focal Lesion Ablative Microboost in Prostate Cancer.
118. ClinicalTrials.gov. Dose Escalation by Boosting Radiation Dose Within the Primary Tumor on the Basis of a Pre-treatment FDG-PET-CT Scan in Stage IB, II and III NSCLC: a Randomized Phase II Trial (PET Boost).
119. Conti M. Focus on time-of-flight PET: the benefits of improved time resolution. *European Journal of Nuclear Medicine and Molecular Imaging*;38:1147-1157.
120. Machtay M, Natwa M, Andrel J*, et al.* Pretreatment FDG-PET standardized uptake value as a prognostic factor for outcome in head and neck cancer. *Head Neck* 2009;31:195-201.
121. Semple SIK, Staff RT, Heys SD*, et al.* Baseline MRI delivery characteristics predict change in invasive ductal breast carcinoma PET metabolism as a result of primary chemotherapy administration. *Annals of Oncology* 2006;17:1393-1398.

Paper I:

Malinen E, Rødal J, Knudtsen IS, Søvik Å, Skogmo HK.

Spatiotemporal analysis of tumor uptake patterns in dynamic ^{18}FDG-PET and dynamic contrast enhanced CT.

Acta Oncologica 2011;50:873-882.

Paper I

Is not included due to copyright

Paper II:

Rødal J, Søvik Å, Skogmo HK, Knudtsen IS, Malinen E.

Feasibility of contrast-enhanced cone-beam CT for target localization and treatment monitoring.

Radiotherapy and Oncology 200;97:521-52

Paper II

Radiotherapy and Oncology 97 (2010) 521–524

Contents lists available at ScienceDirect

Radiotherapy and Oncology

journal homepage: www.thegreenjournal.com

Target definition

Feasibility of contrast-enhanced cone-beam CT for target localization and treatment monitoring

Jan Rødal [a,b,*], Åste Søvik [c,d], Hege Kippenes Skogmo [d], Ingerid Skjei Knudtsen [e], Eirik Malinen [a]

[a] Department of Medical Physics, The Norwegian Radium Hospital, Oslo University Hospital, Norway; [b] Department of Physics, The Norwegian University of Science and Technology, Trondheim, Norway; [c] Department of Radiation Biology, The Norwegian Radium Hospital, Oslo University Hospital, Norway; [d] Department of Companion Animal Clinical Sciences, Norwegian School of Veterinary Science, Oslo, Norway; [e] Interventional Centre, Oslo University Hospital, Norway

ARTICLE INFO

Article history:
Received 19 March 2010
Received in revised form 14 June 2010
Accepted 3 July 2010

Keywords:
Cone-beam CT
Contrast agent
Image guided radiotherapy

ABSTRACT

A dog with a spontaneous maxillary tumour was given 40 Gy of fractionated radiotherapy. At five out of 10 fractions cone-beam CT (CBCT) imaging before and after administration of an iodinated contrast agent were performed. Contrast enhancement maps were overlaid on the pre-contrast CBCT images. The tumour was clearly visualized in the images thus produced.

 Radiotherapy and Oncology 97 (2010) 521–524

Modern linear accelerators with cone-beam CT (CBCT) systems enable volumetric imaging of the patient at the treatment site [1]. Use of bony anatomy, fiducial markers and soft tissue tumours and organs is widely explored as markers for image guided radiotherapy (IGRT) [2–4] and planning [5]. However, using the tumour itself as a registration object is not straightforward. The tumour boundaries may not be visually separable from surrounding soft tissue in an ordinary CBCT image, as reported for head and neck tumours, tumours in the thorax and upper abdomen and in the pelvic region [6,7]. The tumour may also migrate or deform during radiotherapy [8]. Thus, there is a need for methods that improve the soft tissue contrast in CBCT images.

Contrast-enhanced CT with iodinated contrast agents is a common imaging procedure for radiotherapy planning, as soft tissue tumours may show increased enhancement compared to normal tissue due to increased perfusion and blood vessel permeability caused by tumour angiogenesis [9]. The usefulness of contrast-enhanced CBCT imaging has been suggested in the literature [6]. If feasible, such imaging may not only be useful for online/offline patient set-up corrections, but also for monitoring biological and spatial changes of the tumour during treatment [10]. In addition, tumour boosting may be facilitated.

To our knowledge only one group has published results on contrast media-assisted visualization with CBCT [11,12]. In these studies, brain and liver metastases were visualized directly in images acquired after contrast injection. In the current work a different approach was taken, where both pre- and post-contrast images were acquired. Thus, the net contrast enhancement could be obtained voxel by voxel. Overlaid on standard CBCT images this may give improved tumour visualization. Additionally, as contrast-enhanced CBCT imaging was performed during the course of fractionated radiotherapy, a means of monitoring changes in tumour enhancement was provided.

Methods and materials

A nine years old female Border collie with a body weight of 24 kg presented with a spontaneous, 14 cm^3 plasma cell tumour in the right maxilla. The imaging and treatment described below was approved by the National Ethics Committee and a written informed consent was obtained from the dog's owner. Before imaging and treatment, the patient was pre-medicated with detomidin 5 μg/kg iv (Domitor vet., Orion, Turku, Finland) and butorfanol 0.05 mg/kg iv (Dolorex vet., Intervet, Boxmeer, the Netherlands). Anaesthesia was induced with propofol 2.0 mg/kg iv (PropoVet, Abbot, Illinois, USA) and tracheal intubation was performed. Anaesthesia was maintained with continuous rate infusion of propofol at a dose rate of 10 mg/kg/h iv. The patient was placed in prone position on a vacuum cushion (VacFix, Par Scientific A/S, Odense Denmark) in a polymethyl methacrylate (PMMA) case with open front and tail walls. The upper jaw was fixated by a dental form anchored to the PMMA bin.

Three days before start of radiotherapy a PET/CT scan of the dog was obtained at a Biograph16 scanner (Siemens AG, Munich, Germany). The PET/CT images were used as basis for treatment planning (see below). Also, a 10 min dynamic contrast-enhanced CT

* Corresponding author. Address: Department of Medical Physics, The Norwegian Radium Hospital, Oslo University Hospital, Montebello, N-0310 Oslo, Norway.
E-mail address: jan.rodal@radiumhospitalet.no (J. Rødal).

0167-8140/$ - see front matter © 2010 Elsevier Ireland Ltd. All rights reserved.
doi:10.1016/j.radonc.2010.07.006

scan over the central part of tumour was obtained at the same scanner. The contrast uptake in the tumour reached a plateau at about one minute post-injection (PI) (data not shown). The contrast agent was Omnipaque (Iohexol, 300 mg/ml, GE Healthcare, Oslo, Norway), administered intravenously at a dose of 600 mg/kg by means of a power injector.

IMRT was planned using the KonRad inverse treatment planning system (v. 2.2.18, Siemens Medical Solutions, Germany) with five fields, 6 MV photon energy and a dose of 40 Gy over 10 fractions. The patient was treated with curative intent at an Elekta Synergy linear accelerator (Elekta AB, Stockholm, Sweden), equipped with a CBCT system (XVI).

Standard CBCT imaging was performed at each treatment session, and the patient set-up was corrected by automatic bone matching to the reference CT images. Contrast-enhanced CBCT imaging with Omnipaque 300 mg/ml at a dose of 600 mg/kg was performed at five of the treatment sessions (Nos. 1, 3, 5, 7 and 10). At these sessions a CBCT scan was taken immediately before manual contrast injection, and a second scan was started one minute PI. No repositioning was permitted between pre- and post-contrast CBCT scans.

Axial CBCT images were reconstructed in the XVI system from the volumetric uptakes. The reconstructed slice thickness was 1 mm and the image size 512×512 pixels with pixel size 1 mm. The images were analyzed using custom made software in IDL (ITT Visual Information Solutions, Boulder, USA). Briefly, the pre-contrast images were subtracted from the post-contrast images. As contrast was injected manually, variations between fractions in injection time and injected volume could be an issue. Indeed, some contrast was spilled at one session (fraction 7). To correct for such irregularities the subtraction images were normalized according to normal tissue enhancement at the first session. The subtraction images were scaled using a window level of 100 Hounsfield units (HU) and a window width of 100 HU. The resulting images were overlaid on the pre-contrast CBCT images. A 'red temperature' colour gradient was used for displaying the enhancement image in the overlay. The same procedure was performed for the contrast-enhanced pre-treatment conventional CT images, with a window level/width setting of 90/85 HU.

Treatment monitoring was tentatively performed by calculating the mean contrast enhancement in the tumour at each session. A region of interest (ROI) for scoring the enhancement was defined inside the tumour in pre-treatment CBCT images, with a few pixels margin to the tumour border. The same ROI was used for all five sessions where contrast-enhanced CBCT was performed.

Results

The maxillary tumour was clearly presented in the contrast-enhanced overlay CT and CBCT images. A comparison of conventional CT, CBCT and PET/CT overlays is shown in Fig. 1. The tumour extent and orientation appeared very similar in the respective images. Using contrast-enhanced CBCT the tumour was clearly discriminated throughout the fractionated treatment (Fig. 2).

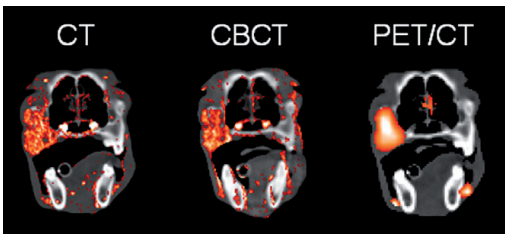

Fig. 1. Left: Conventional CT with contrast enhancement overlay. Middle: CBCT with contrast enhancement overlay. Right: Conventional CT with FDG-PET overlay. High uptake/enhancement is indicated by bright colours. The CT and PET/CT images are taken three days before treatment start, the CBCT image is taken prior to the first treatment.

A slight increase in tumour enhancement during the treatment may be seen and the mean contrast enhancement in the tumour ROI was calculated. Following first order linear regression, a significant ($P < 0.01$) increase in contrast enhancement of 5.2 HU per treatment fraction was found. The standard deviation in tumour contrast enhancement (indicating intra tumour heterogeneity) varied from 29 to 46 HU between the fractions.

Discussion

Angiogenesis is essential for tumour growth and alters contrast enhancement during CT [9]. Contrast-enhanced CT is thus a modality which may be a marker for tumour tissue, as is the case for FDG-PET [13]. The present work aimed at exploring contrast-enhanced CBCT for highlighting tumour tissue. For the actual canine patient, the tumour was clearly discriminated from its surroundings using both contrast-enhanced CT, FDG-PET and contrast-enhanced CBCT. Therefore, contrast-enhanced CBCT may be used to identify the tumour position during treatment, which may be utilized separately or in combination with bony anatomy registering. The basis for such tumour tissue matching should be pre-treatment contrast-enhanced CT or contrast-enhanced MR images, processed with the same procedure to establish reference tumour shape and size. The method could be particularly useful when treating extracranial lesions where the spatial relation between the tumour region and superficial skin markers or bony anatomy is weakly correlated [14,15].

Another utilization of contrast-enhanced CBCT is to detect spatial or functional tumour changes along the treatment course without taking the patient through additional CT or MRI surveys. The location, shape and size of tumours have been found to change significantly during the treatment course due to tumour shrinkage, weight loss and other factors [8,16,17]. Spatial changes can potentially be assessed by extracting the enhanced volume, as shown in the current work. Functional changes can be revealed by analyzing the degree of enhancement within the tumour, which indicate radiation-induced changes in tumour functionality. This was demonstrated in the present case, where increased contrast enhancement during the treatment course was found.

The cost of obtaining improved spatial and functional information is an additional contrast-enhanced CBCT scan at selected treatment sessions. This has drawbacks, such as prolonged treatment sessions, injection of contrast agent and increased X-ray dose to the patient. These aspects must be considered when adapting the technique to human patients. In particular, contrast-induced nephropathy (CIN) is a matter of great concern, and diabetes, reduced renal function and old age are among the risk factors [18]. CT contrast can also interact with certain drugs [18]. Tumour boosting based on contrast-enhanced CBCT once or twice a week might provide a high local control rate, as indicated in our previous work employing biologically adapted treatment planning [19]. However, the risk of CIN and other adverse reactions limit the number of contrast-enhanced CBCT sessions, and frequent contrast-enhanced CBCT imaging might be controversial. Possible adverse effects of repeated administration of contrast media were addressed in a study investigating a novel CT/MRI contrast agent of liposomes co-encapsulating iohexol and gadoteridol [20]. The novel formulation may provide long-lasting contrast enhancement in the tumour with a decreased risk of toxicity. In any case, clinical trials employing serial contrast-enhanced imaging (with established or novel contrast media) must include examinations aimed

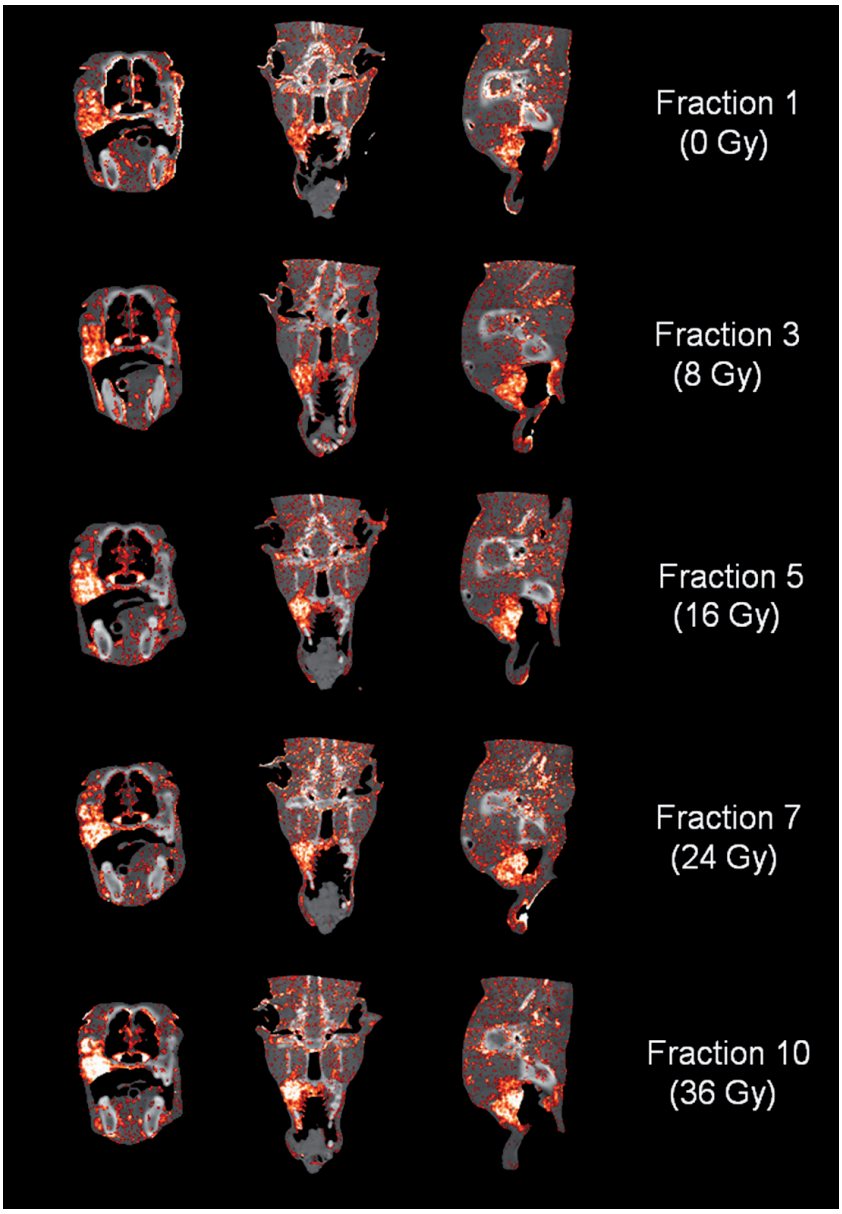

Fig. 2. Reconstructed CBCT images in three planes with contrast enhancement overlay at five treatment fractions. High uptake/enhancement is indicated by bright colours.

at revealing contraindications, in addition to regular follow-up of acute and long-term side effects.

In a clinical setting, injecting the contrast medium with a power injector would be preferred in favour of a manual procedure, as was used in the current work. A power injector ensures reduced injection time and more reproducible timing of the contrast administration. This may reduce the need for normalizing the images, which was done here due to possible variations in contrast administration throughout the course of treatment.

In the present case the tumour was significantly enhanced compared to the surrounding normal tissues (Figs. 1 and 2). However, normal tissue uptake and statistical noise from the XVI system are also visible in the overlay images. The noise may be reduced by applying a smoothing filter, which should be optimized against

the corresponding degradation of the tumour signal. Also, the subtraction procedure (pre-contrast from post-contrast) for producing the enhancement image is sensitive to shift errors, creating edge artefacts in the overlay images. This can be seen in the images in Fig. 2 as enhancements along the rim of bony structures. Such artefacts could arise even with our sedated patient due to minor spatial disturbances, possibly induced by the contrast injection. For a human, non-sedated patient this will be even more pertinent, where patient motion in the order of millimetres may occur. Provided no internal tumour movement between pre- and post-contrast CBCT however, precise coregistration of the image sets can reduce or eliminate these artefacts. The coregistration can be done using bony anatomy or fiducial markers [21] close to the tumour in the pre- and post-contrast data sets, thereby generating translation and rotation parameters to adjust the image sets. This technique is well established in today's commercial cone-beam systems and could be implemented in the current application as well.

In contrast to conventional CT, where the gantry rotation time is in the order of one second, the duration of the currently used CBCT scan is typically one minute. The underlying contrast kinetics for the CBCT images will therefore be averaged over this scan time. The conventional CT images in Fig. 1 were derived 2 min PI, and correspond approximately to the situation at the end of the CBCT scan. A complete resemblance between images produced by the two CT modalities may not be obtained, however, due to the differences in scan time, detector and beam technologies and reconstruction algorithms. Still, the tumour appeared qualitatively congruent in the images presented in Fig. 1.

In conclusion, this work showed that contrast-enhanced CBCT is feasible and may prove valuable for radiation oncology. The method is clinically relevant, but refinement and further research are required to make the procedure clinically applicable.

Acknowledgement

Professor Arne Skretting is acknowledged for the support with PET/CT imaging.

References

[1] Jaffray DA, Siewerdsen JH, Wong JW, Martinez AA. Flat-panel cone-beam computed tomography for image-guided radiation therapy. Int J Radiat Oncol Biol Phys 2002;53:1337–49.
[2] Smitsmans MHP, de Bois J, Sonke JJ, Betgen A, Zijp LJ, Jaffray DA, et al. Automatic prostate localization on cone-beam CT scans for high precision image-guided radiotherapy. Int J Radiat Oncol Biol Phys 2005;63:975–84.
[3] Letourneau D, Martinez AA, Lockman D, Yan D, Vargas C, Ivaldi G, et al. Assessment of residual error for online cone-beam CT-guided treatment of prostate cancer patients. Int J Radiat Oncol Biol Phys 2005;62:1239–46.
[4] Dawson LA, Jaffray DA. Advances in image-guided radiation therapy. J Clin Oncol 2007;25:938–46.
[5] Oldham M, Letourneau D, Watt L, Hugo G, Yan D, Lockman D, et al. Cone-beam-CT guided radiation therapy: a model for on-line application. Radiother Oncol 2005;75:271–8.
[6] Higgins J, Bezjak A, Franks K, Le LW, Cho BC, Payne D, et al. Comparison of spine, carina, and tumor as registration landmarks for volumetric image-guided lung radiotherapy. Int J Radiat Oncol Biol Phys 2009;73:1404–13.
[7] McBain CA, Henry AM, Sykes J, Amer A, Marchant T, Moore CM, et al. X-ray volumetric imaging in image-guided radiotherapy: the new standard in on-treatment imaging. Int J Radiat Oncol Biol Phys 2006;64:625–34.
[8] Mohan R, Zhang XD, Wang H, Kang YX, Wang XC, Liu H, et al. Use of deformed intensity distributions for on-line modification of image-guided IMRT to account for interfractional anatomic changes. Int J Radiat Oncol Biol Phys 2005;61:1258–66.
[9] Miles KA. Tumour angiogenesis and its relation to contrast enhancement on computed tomography: a review. Eur J Radiol 1999;30:198–205.
[10] Jaffray D, Kupelian P, Djemil T, Macklis RM. Review of image-guided radiation therapy. Expert Rev Anticancer Ther 2007;7:89–103.
[11] Nakagawa K, Yamashita H, Igaki H, Terahara A, Shiraishi K, Yoda K. Contrast medium-assisted stereotactic image-guided radiotherapy using kilovoltage cone-beam computed tomography. Radiat Med 2008;26:570–2.
[12] Igaki H, Nakagawa K, Yamashita H, Terahara A, Haga A, Shiraishi K, et al. Contrast media-assisted visualization of brain metastases by kilovoltage cone-beam CT. Acta Oncol 2009;48:314–7.
[13] Frank SJ, Chao KSC, Schwartz DL, Weber RS, Apisarnthanarax S, Macapinlac HA. Technology insight: PET and PET/CT in head and neck tumor staging and radiation therapy planning. Nat Clin Pract Oncol 2005;2:526–33.
[14] Ploeger LS, Betgen A, Gilhuijs KGA, van Herk M. Feasibility of geometrical verification of patient set-up using body contours and computed tomography data. Radiother Oncol 2003;66:225–33.
[15] Zelefsky MJ, Crean D, Mageras GS, Lyass O, Happersett L, Ling CC, et al. Quantification and predictors of prostate position variability in 50 patients evaluated with multiple CT scans during conformal radiotherapy. Radiother Oncol 1999;50:225–34.
[16] McDermott LN, Wendling M, Sonke JJ, van Herk M, Mijnheer BJ. Anatomy changes in radiotherapy detected using portal imaging. Radiother Oncol 2006;79:211–7.
[17] Erridge SC, Seppenwoolde Y, Muller SH, van Herk M, De Jaeger K, Belderbos JSA, et al. Portal imaging to assess set-up errors, tumor motion and tumor shrinkage during conformal radiotherapy of non-small cell lung cancer. Radiother Oncol 2003;66:75–85.
[18] Hasebroock KM, Serkova NJ. Toxicity of MRI and CT contrast agents. Expert Opin Drug Metab Toxicol 2009;5:403–16.
[19] Sovik A, Malinen E, Skogmo HK, Bentzen SM, Bruland OS, Olsen DR. Radiotherapy adapted to spatial and temporal variability in tumor hypoxia. Int J Radiat Oncol Biol Phys 2007;68:1496–504.
[20] Zheng JZ, Liu JB, Dunne M, Jaffray DA, Allen C. In vivo performance of a liposomal vascular contrast agent for CT and MR-based image guidance applications. Pharm Res 2007;24:1193–201.
[21] Sovik A, Malinen E, Olsen DR. Strategies for biologic image-guided dose escalation: a review. Int J Radiat Oncol Biol Phys 2009;73:650–8.

Paper III:

Søvik Å, Rødal J, Skogmo HK, Lervåg C, Eilertsen K, Malinen E.

Adaptive radiotherapy based on contrast enhanced cone-beam CT imaging.

Acta Oncologica 2010;49:972-977.

Paper III

Is not included due to copyright

Paper IV:

Rødal J, Søvik Å, Malinen E.

Influence of MLC leaf width on biologically adapted IMRT plans.

Acta Oncologica 2010;49:1116-1123.

Paper IV

Is not included due to copyright

Paper V:

Rødal J, Waldeland E, Søvik Å, Malinen, E.

Dosimetric verification of biologically adapted IMRT.

Medical Physics 2011;38:2586-2594.

Paper V

Is not included due to copyright